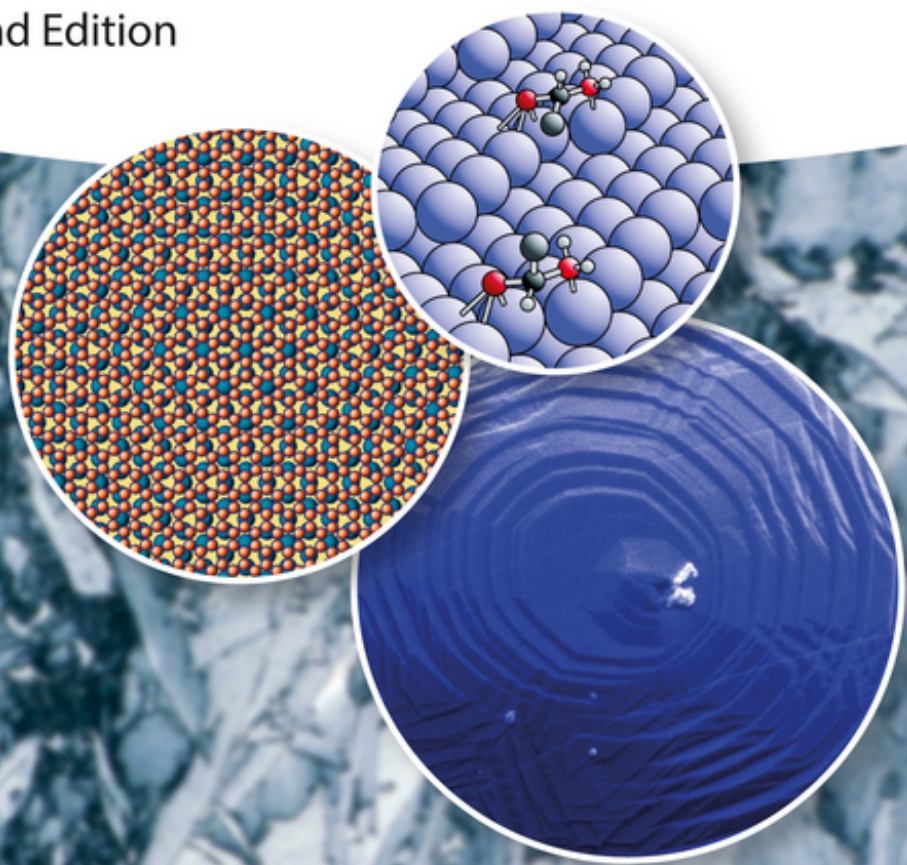


Klaus Hermann

# Crystallography and Surface Structure

An Introduction for Surface  
Scientists and Nanoscientists

Second Edition





*Klaus Hermann*

**Crystallography and Surface Structure**



*Klaus Hermann*

# **Crystallography and Surface Structure**

An Introduction for Surface Scientists and Nanoscientists

*Second, Revised and Expanded Edition*

**WILEY-VCH**  
Verlag GmbH & Co. KGaA

#### Author

*Prof. Dr. Klaus Hermann*  
Fritz-Haber-Institut der MPG  
Theory Department  
Faradayweg 4-6  
14195 Berlin  
Germany

#### Cover

The book cover includes a scanning electron microscopy picture of a stepped Cu<sub>2</sub>O surface (large circular area), kindly provided by Marc Willinger, Fritz-Haber Institute Berlin.

Medium circle: Interference structure of graphene on iridium, theory.

Small circle: Simulation of chiral molecules at a stepped surface.

All books published by **Wiley-VCH** are carefully produced. Nevertheless, authors, editors, and publisher do not warrant the information contained in these books, including this book, to be free of errors. Readers are advised to keep in mind that statements, data, illustrations, procedural details or other items may inadvertently be inaccurate.

**Library of Congress Card No.:** applied for

#### **British Library Cataloguing-in-Publication Data**

A catalogue record for this book is available from the British Library.

#### **Bibliographic information published by the Deutsche Nationalbibliothek**

The Deutsche Nationalbibliothek lists this publication in the Deutsche Nationalbibliografie; detailed bibliographic data are available on the Internet at <<http://dnb.d-nb.de>>.

© 2017 Wiley-VCH Verlag GmbH & Co. KGaA, Boschstr. 12, 69469 Weinheim, Germany

All rights reserved (including those of translation into other languages). No part of this book may be reproduced in any form – by photoprinting, microfilm, or any other means – nor transmitted or translated into a machine language without written permission from the publishers. Registered names, trademarks, etc. used in this book, even when not specifically marked as such, are not to be considered unprotected by law.

**Print ISBN:** 978-3-527-33970-9

**ePDF ISBN:** 978-3-527-69712-0

**ePub ISBN:** 978-3-527-69714-4

**Mobi ISBN:** 978-3-527-69715-1

**oBook ISBN:** 978-3-527-69713-7

**Cover Design** Grafik-Design Schulz  
**Typesetting** SPi Global, Chennai, India  
**Printing and Binding**

Printed on acid-free paper

## Contents

**Preface to the Second Edition** *IX*

**Preface to the First Edition** *XI*

<b>1</b>	<b>Introduction</b>	<i>1</i>
<b>2</b>	<b>Bulk Crystals: Three-Dimensional Lattices</b>	<i>7</i>
2.1	Basic Definition	<i>7</i>
2.2	Representation of Bulk Crystals	<i>11</i>
2.2.1	Alternative Descriptions Conserving the Lattice Representation	<i>12</i>
2.2.2	Alternative Descriptions Affecting the Lattice Representation	<i>14</i>
2.2.2.1	Cubic, Hexagonal, and Trigonal Lattices	<i>16</i>
2.2.2.2	Superlattices and Repeated Slabs	<i>25</i>
2.2.2.3	Linear Transformations of Lattice Vectors	<i>29</i>
2.2.3	Centered Lattices	<i>31</i>
2.3	Periodicity Cells of Lattices	<i>35</i>
2.4	Lattice Symmetry	<i>38</i>
2.5	Reciprocal Lattice	<i>49</i>
2.6	Neighbor Shells	<i>52</i>
2.7	Nanoparticles and Crystallites	<i>63</i>
2.8	Incommensurate Crystals and Quasicrystals	<i>71</i>
2.8.1	Modulated Structures	<i>71</i>
2.8.2	Incommensurate Composite Crystals	<i>73</i>
2.8.3	Quasicrystals	<i>76</i>
2.9	Exercises	<i>82</i>
<b>3</b>	<b>Crystal Layers: Two-Dimensional Lattices</b>	<i>91</i>
3.1	Basic Definition, Miller Indices	<i>91</i>
3.2	Netplane-Adapted Lattice Vectors	<i>96</i>
3.3	Symmetrically Appropriate Lattice Vectors: Minkowski Reduction	<i>98</i>
3.4	Miller Indices for Cubic and Trigonal Lattices	<i>100</i>
3.5	Alternative Definition of Miller Indices and Miller–Bravais Indices	<i>106</i>

3.6	Symmetry Properties of Netplanes	109
3.6.1	Centered Netplanes	110
3.6.2	Inversion	111
3.6.3	Rotation	114
3.6.4	Mirror Operation	119
3.6.5	Glide Reflection	131
3.6.6	Symmetry Groups	139
3.7	Crystal Systems and Bravais Lattices in Two Dimensions	144
3.8	Crystallographic Classification of Netplanes and Monolayers	149
3.8.1	Oblique Netplanes	151
3.8.2	Primitive Rectangular Netplanes	151
3.8.3	Centered Rectangular Netplanes	155
3.8.4	Square Netplanes	157
3.8.5	Hexagonal Netplanes	158
3.8.6	Classification Overview	163
3.9	Exercises	164
<b>4</b>	<b>Ideal Single Crystal Surfaces</b>	<b>169</b>
4.1	Basic Definition, Termination	169
4.2	Morphology of Surfaces, Stepped and Kinked Surfaces	175
4.3	Miller Index Decomposition	178
4.4	Chiral and Achiral Surfaces	192
4.5	Exercises	204
<b>5</b>	<b>Real Crystal Surfaces</b>	<b>209</b>
5.1	Surface Relaxation	209
5.2	Surface Reconstruction	210
5.3	Growth Processes	222
5.4	Faceting	226
5.5	Exercises	231
<b>6</b>	<b>Adsorbate Layers</b>	<b>235</b>
6.1	Definition and Classification	235
6.2	Adsorbate Sites	241
6.3	Wood Notation of Surface Structure	251
6.4	High-Order Commensurate (HOC) Overlayers	258
6.5	Interference Lattices	263
6.5.1	Basic Formalism	264
6.5.2	Interference and Wood Notation	272
6.5.3	Anisotropic Scaling, Stretching, and Shifting	279

6.6	Symmetry and Domain Formation	283
6.7	Adsorption at Surfaces and Chirality	293
6.8	Exercises	299
<b>7</b>	<b>Experimental Analysis of Real Crystal Surfaces</b>	<b>305</b>
7.1	Experimental Methods	305
7.2	Surface Structure Compilations	306
7.3	Database Formats for Surface and Nanostructures	311
7.4	Exercises	313
<b>8</b>	<b>Nanotubes</b>	<b>315</b>
8.1	Basic Definition	315
8.2	Nanotubes and Symmetry	319
8.3	Complex Nanotubes	323
8.4	Exercises	326
	<b>Appendix A: Sketches of High-Symmetry Adsorbate Sites</b>	<b>329</b>
A.1	Face-Centered Cubic (fcc) Surface Sites	330
A.2	Body-Centered Cubic (bcc) Surface Sites	338
A.3	Hexagonal Close-Packed (hcp) Surface Sites	342
A.4	Diamond Surface Sites	346
A.5	Zincblende Surface Sites	349
	<b>Appendix B: Parameter Tables of Crystals</b>	<b>351</b>
	<b>Appendix C: Mathematics of the Wood Notation</b>	<b>355</b>
C.1	Basic Formalism and Examples	355
C.2	Wood-Representability	361
	<b>Appendix D: Mathematics of the Minkowski Reduction</b>	<b>367</b>
	<b>Appendix E: Details of Number Theory</b>	<b>371</b>
E.1	Basic Definitions and Functions	371
E.2	Euclid's Algorithm	376
E.3	Linear Diophantine Equations	377
E.4	Quadratic Diophantine Equations	380
E.5	Number Theory and $2 \times 2$ Matrices	386
	<b>Appendix F: Details of Vector Calculus and Linear Algebra</b>	<b>391</b>
	<b>Appendix G: Details of Fourier Theory</b>	<b>395</b>
	<b>Appendix H: List of Surface Web Sites</b>	<b>399</b>

**Appendix I: List of Surface Structures** 401

**Glossary and Abbreviations** 403

**References** 417

**Index** 425

## Preface to the Second Edition

As a result of feedback from readers of the first edition of this book and from colleagues, this second edition is a major revision that goes beyond mere error correction and minor clarification. While the book has been modified and extended greatly, the initial concept of a combined tutorial introduction into surface crystallography, with bulk crystallography as a basis, and an overview of modern subjects for the advanced researcher has been conserved. Many sections have been updated for completeness and have been extended to include recent developments due to the advent of new and more refined measuring techniques.

The second edition is also targeted at researchers working on graphene and other weakly adsorbing overlayers that form large size moiré patterns observed by scanning tunneling and electron microscopy. They might appreciate the new section on moiré lattice formation, which until now has not been available in any textbook format. Nanoparticle physicists and materials scientists who are interested in structure information of very small particles and seek to connect, for example, electronic and magnetic properties with structural data, may benefit from the sections on nanoparticles, crystal spheres, nanotubes, as well as faceting. This might also interest catalytic chemists trying to interpret chemical behavior, such as reactivity, by structural information of small particles.

Specific items that have been newly added or revised include

- nanoclusters and crystallites, giving a basic overview on structure details;
- incommensurate and quasicrystals, being treated on a common basis;
- basics of epitaxy and crystal growth;
- further details on chiral surfaces and adsorbates;
- the theoretical treatment of high-order commensurate (HOC) overlayers;
- the theory of interference lattices and moiré patterns;
- the geometric structure of high-symmetry adsorbate sites;
- more detailed computational algorithms in the appendices; and
- structure database formats, documenting measured surface structures.

Furthermore, the list of references to original publications and books on specific subjects has been revised and extended to account for more recent experimental and theoretical developments. The set of exercises that conclude each section has

been substantially enlarged following suggestions by readers of the first book edition. All structure graphics in this book have been created using the interactive software *Balsac* (Build and Analyze Lattices, Surfaces, And Clusters) developed by the author ((C) K. Hermann, Fritz-Haber-Institut, Berlin, 1990–2016).

Michel A. Van Hove and Wolfgang Moritz have once again lent invaluable support through their constructive criticism and detailed suggestions. I am particularly indebted to Michel for our fruitful discussions during various extended research visits to the Institute of Computational and Theoretical Studies (ICTS) at Hong Kong Baptist University, which have helped to improve the revised text in innumerable ways. Advice from other colleagues on subjects specific to the second edition has likewise been instrumental in improving this edition, as also the suggestions on interference lattices by Michael S. Altman, on growth mechanisms by Ernst G. Bauer, on quasicrystals by Renee D. Diehl, and on chirality by Andrew J. Gellman and Rasmita Raval. Critical reading of the final manuscript by Travis Jones and color design advice on figures by Liudmyla Masliuk are greatly acknowledged.

Finally, unsurpassed support and overwhelming patience by my wife Hanna has again proven essential for the completion of this book project.

Fritz-Haber-Institut, Berlin  
Autumn 2015

*Klaus Hermann*

## Preface to the First Edition

The objective of this book is to provide students and researchers with the crystallographic foundations necessary to understand the structure and symmetry of surfaces and the interfaces of crystalline materials. This includes macroscopic single crystals as well as crystalline nanoparticles. Knowledge of their geometric properties is a prerequisite for the interpretation of corresponding experimental and theoretical results, which explain both their physical and chemical behavior. In particular, surface and interface structure is of vital importance not only for the study of properties near single crystal surfaces, but also for research on thin films at solid substrates. Here, technological applications range from semiconductor devices and magnetic storage disks to heterogeneous catalysts.

Crystalline nanoparticles, such as nanotubes, nanowires, or compact particles of finite size have recently attracted considerable interest due to their novel chemical and physical properties. Examples are carbon nanotubes, silicon nanowires, nanosize quantum dots at semiconductor surfaces, or catalytically active crystallites. These particles are of finite size in one or more dimensions, but their local atom arrangement can still be close to that of extended bulk crystals. In addition, their surfaces and interfaces with other material can be described analogously to those found for single crystal surfaces. Thus, surface crystallography, covered in this book, can also be applied for the analysis of structural properties of nanoparticle surfaces.

While treatises on three-dimensional crystallography are abundant, there are only few chapters on surface crystallography that are available in specialized surface science reviews. In particular, comprehensive textbooks on surface structure have not yet been published. Nevertheless, students and researchers entering the field need to obtain a thorough overview of surface structure and geometry, which includes all relevant basic crystallographic methods required for theoretical and experimental analyses. This book tries to serve this purpose. It is primarily meant for graduate and PhD students in physics, chemistry, and crystallography, but will also help researchers who want to learn more details about geometric structure at surfaces of single crystals or nanoparticles.

The book is written by a theoretical surface scientist. Therefore, the discussion of methods and approaches in the text is frequently adapted to surfaces and differs in some places from traditional treatment of crystallography. As an example,

number theoretical methods are used to derive appropriate transformations between equivalent lattice descriptions. Further, some of the conventional surface structure concepts are looked at from a different perspective and go beyond the standard treatment that is practiced inside the surface science community. Examples are the introduction of Miller indices based on netplane-adapted lattices and a thorough mathematical treatment of symmetry, which results in the 17 two-dimensional space groups. Therefore, the text can also be used as a resource that is complementary to the standard surface science literature.

This book started as a manuscript of a series of lectures on surface crystallography, given by the author at several international workshops and in universities as well as in research institutions where surface science and catalysis groups were engaged in research on the structural properties of surfaces. Questions and discussions during the lectures were often the source for more detailed work on different sections of the manuscript and thus helped to improve its presentation. Furthermore, research visits to various surface science groups raised the author's awareness of new or incompletely treated issues that had to be dealt with. The author is indebted to all those who contributed with their scientific curiosity and criticism. The text has benefited from numerous discussions with surface scientists, crystallographers, and mathematicians of whom only a few are mentioned in alphabetic order: Gerhard Ertl, Klaus Heinz, Bernhard Hornfeck, Klaus Müller, John B. Pendry, Gabor A. Somorjai, D. Phil Woodruff. Wolfgang Moritz served as an extremely valuable sparring partner in the world of crystallography. Very special thanks go to Michel A. Van Hove whose constructive criticism, rich ideas, and continuous support during the writing phase were unmatched. Without him the book would not exist in its present form.

Finally, I am greatly indebted to my wife Hanna for her patience and loving care throughout the time it took to finish this book and beyond.

Fritz-Haber-Institut, Berlin  
Summer 2010

*Klaus Hermann*

# 1

## Introduction

Research in many areas of materials science requires detailed knowledge about crystalline solids on an atomic scale. These systems may represent real materials such as complex semiconductors, or may act as meaningful models, for example, by simulating reactive sites of catalysts. Here, physical and chemical insight depends very much on the details of the geometric structure of local environments of atoms and of the possible periodic atom arrangements inside the crystal as well as at its surface. As examples we mention the following:

- **Chemical binding** between atoms inside a crystal but also at its surfaces depends, apart from atomic parameters, strongly on local geometry [1, 2]. This is very often expressed by local **coordination** that describes the number and arrangement of nearest neighbor atoms with respect to the binding atom. As an example, metal atoms inside a bulk metal crystal are usually characterized by a large number of nearest neighbors, 8 or 12, yielding metallic binding. At surfaces, the change in chemical binding due to different coordination, compared with that inside the bulk, is tightly connected with local structure, which can be expressed by relaxation and reconstruction. Further, atoms or molecules can adsorb at specific sites of crystalline substrates, where the adsorption geometry is essential for understanding their local binding behavior.
- **Electronic properties** at surfaces of single crystals can differ substantially from those of the corresponding bulk. For example, the existence of a surface can induce additional electronic states, so-called surface states, that have been found in experiments and studied theoretically for some time [3]. Here, the detailed surface structure determines the existence as well as the energetic behavior of the states. Further, electronic interband transitions in silicon nanowires and nanodots are found to cause photoluminescence that does not occur in silicon bulk crystals [4]. The difference is explained by both the spatial confinement of the nanoparticles and also by changes in geometric properties of their atom arrangement. Finally, it has been claimed from experiments that semiconducting bulk silicon shows metallicity at its  $(7 \times 7)$  reconstructed  $(1\ 1\ 1)$  surface [5], and metallicity is also found in theoretical studies on silicon nanowires [6].

- **Magnetism** of crystalline bulk material as well as of its surfaces depends on the crystal structure and local coordination. For example, vanadium sesquioxide,  $V_2O_3$ , in its monoclinic crystal structure is antiferromagnetic at low temperatures, whereas its high-temperature phase, described by a trigonal corundum lattice, is paramagnetic [7]. Vanadium crystals with a body-centered cubic lattice are found to be paramagnetic in their bulk volume but ferromagnetic at their surfaces [8]. Other examples are thin iron films grown on top of copper single crystal surfaces where, as a function of film thickness, their crystal structure changes and, as a consequence, their magnetic properties [9].
- **Anisotropic electrical conductivity** is often connected with dense atom packing along specific directions inside a crystal. An example is given by trigonal  $LiCoO_2$  crystals that form the most common lithium storage material for rechargeable batteries. Here, the electrical conductivity is greatly enhanced along densely packed Co and Li planes while it is much smaller perpendicular to the planes [10].
- **Catalytic surface reactions** depend crucially on structural properties of the surfaces of crystalline catalyst materials at an atomic scale [11, 12]. The atomic surface structure determines possible adsorption and reaction sites for molecules, which can support specific catalytic reactions but can also exclude others known as *structure–reactivity relationships* [11]. For example, catalytic CO oxidation happens at single crystal surfaces of platinum with different efficiency depending on the surface orientation [13], where the surface structure determines the type and density of reactive sites.

In addition to bulk crystals and their surfaces, studies on crystalline **nanoparticles** [14, 15] have become an exciting field of research. This includes nanotubes [16], nanowires [14], or compact particles of finite size, such as atom clusters [17], fullerenes [18], or quantum dots [19], which show novel physical and chemical properties deviating from those of the corresponding bulk material. Examples are carbon nanotubes providing substrate material to yield new active catalysts [20] or silicon nanowires whose visible photoluminescence is determined by their size [21]. Further, nanosize quantum dots at semiconductor surfaces are found to yield quite powerful light emitting diodes (LEDs) of technological relevance [19].

These nanoparticle systems are described as **atom aggregates** of finite size in one or more dimensions, where their local geometric arrangement can still be close to that of extended bulk crystals. Likewise, their spatial confinement with corresponding surfaces and interfaces can be considered analogous to that appearing at bulk crystal surfaces. Therefore, surface crystallography, initially developed to describe structural properties at single crystal surfaces, also forms a sound basis by which the structure of nanoparticle surfaces can be characterized. This is particularly interesting since the relative number of atoms positioned at nanoparticle surfaces compared with those of their inner volume is always larger than that of extended macroscopic single crystals. Thus, the relative importance of atoms at **nanoparticle surfaces** in determining physical properties is expected to be greater than that of atoms at single crystal surfaces. In addition, nanoparticles

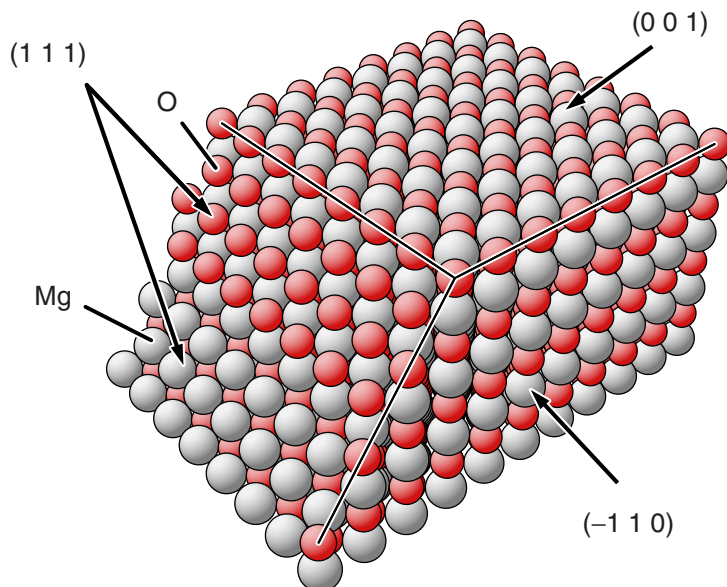


**Figure 1.1** Section of an MgO crystal (NaCl lattice). The atoms are shown as shaded balls of different color and labeled accordingly. The section is enclosed by nonpolar (0 0 1), (−1 1 0), and by polar (1 1 1) oriented surfaces.

can possess symmetry and geometric properties that do not appear in single crystals or at their surfaces. Examples are icosahedral clusters or curved nanoparticle surfaces that originate from bending single crystal sections, where in this book **nanotubes** will be discussed as examples.

In many experimental and theoretical studies real crystalline systems are, for the sake of simplicity, approximately described as **ideal single crystals** with a well-defined atomic composition and an unperturbed three-dimensional periodicity. In addition, planar surfaces of single crystals are often assumed to be bulk-terminated and of unperturbed two-dimensional periodicity. With this approximation in mind a rigorous mathematical description of all structural parameters becomes possible and is one of the basic subjects of classical crystallography. As an illustration, Figure 1.1 shows the structure of a section of an ideal single crystal of magnesium oxide, MgO, with its perfect three-dimensional periodic arrangement of atoms. Here, sections of ideal planar surfaces, originating from bulk truncation, become visible and demonstrate the variety of surface types for the same crystal depending on the crystal cut.

In the following chapters of this book we will discuss the basic elements as well as the **mathematical methods** used in crystallography to evaluate structural parameters of single crystals with particular emphasis on their surfaces. We start with ideal bulk crystals of three-dimensional periodicity, where classical bulk crystallography provides a quantitative description. Then we introduce ideal two-dimensional surfaces as a result of bulk truncation along specific directions

including high density, vicinal, stepped, kinked, and chiral surfaces. We give a detailed account of their two-dimensional symmetry behavior following the crystallographic classification scheme of Bravais lattices and two-dimensional space groups. Next, we discuss details of the deviation of atomic structures at surfaces due to changes in surface binding compared with that in the bulk. This is usually described by surface relaxation and reconstruction, where we consider different schemes. In addition, structural behavior during growth processes is discussed. Then we deal with the crystallographic aspects of commensurate, high-order commensurate, and incommensurate adsorbate systems as special cases of surface reconstruction. Here also the different structure notations used in the literature will be described. The discussion of surface structure will be completed by an overview of the surfaces that have been analyzed quantitatively at an atomic level in scattering, diffraction, imaging, or spectroscopic experiments. Further, formal requirements of complete quantitative surface structure databases will be considered. Finally, we describe the theoretical aspects and structural details of nanotubes of different element composition as special cases of rolled sections of crystal monolayers. These nanotubes are examples of a larger class of crystalline materials, nanoparticles mentioned above, and demonstrate that crystallographic methods can also be applied to these systems in order to account for their structural properties. Finally, the book concludes with appendices spelling out further details of the mathematical methods used in the different sections, with tabulations of typical surface sites, and with compilations of structural parameters of crystals.

The theoretical concepts treated in this book will be illustrated by example applications for further understanding, which include results from **measured** real single crystal surfaces documented in the Surface Structure Database (**SSD**) [22–24] or its earlier version **SCIS** (Surface Crystallographic Information Service) [25]. In addition, each chapter of the book concludes with a set of **exercises**. These exercises are of varying difficulty, ranging from simple questions to small research projects, and are meant to stimulate the discussion on the different subjects and to contribute to their clarification. Some of the exercises may require **visualization tools** for crystals, such as **Balsac** [26] or **Survivis** [27] or the like.

In the theoretical treatment of some structural properties of ideal single crystals we will apply **number theoretical methods**, dealing with relations between integers. While this approach is not commonly used in textbooks on surface science or crystallography it can simplify the formal treatment considerably. Examples are solutions of linear and quadratic Diophantine equations that facilitate the discussion of monolayers or of atom neighbor shells in crystals. Therefore, number theoretical methods will be introduced briefly as required and further details are found in Appendix E.

A few illustrations are included as **stereo pictures** for an enhanced three-dimensional impression. These pictures may be viewed either by using optical stereo glasses (available separately) or by cross-eyed viewing without glasses.

In the latter case, viewing for an extended time may overstrain the eyes and should be avoided.

Clearly, the present book cannot cover all aspects of the field and may, in some cases, be quite brief. Further, the selection of topics as well as their presentation is, to some degree, determined by the author's personal preferences. However, the interested reader is referred to the extensive crystallographic literature, see for example, [28–33], to the surface science literature, see for example, [34–39], or to the solid state physics literature, see for example, [1, 2, 40], to explore additional details.



## 2 Bulk Crystals: Three-Dimensional Lattices

This section deals with the geometric properties of three-dimensional **bulk crystals**, which are described, in their perfect structure, by atom arrangements that are periodic in three dimensions. As an example, Figure 2.1 shows a section of a tetragonal  $\text{YBa}_2\text{Cu}_3\text{O}_7$  crystal, where vectors  $\underline{R}_1$ ,  $\underline{R}_2$ ,  $\underline{R}_3$  (lattice vectors) indicate the mutually perpendicular directions of periodicity. Further, the basis of the crystal structure consists of 13 atoms (1  $\times$  yttrium, 2  $\times$  barium, 3  $\times$  copper, 7  $\times$  oxygen) inside a rectangular block (unit cell) that is repeated periodically inside the crystal. The building unit is shown to the left of the figure.

In this section, all **basic definitions** used for a quantitative description of structural properties of perfect three-dimensionally periodic crystals will be provided. Here, the crystals are considered not only in terms of their translational symmetry, that is, periodicity, but also by their different point symmetry elements, such as inversion points, mirror planes, or rotation axes, which characterize the positions of all atoms inside a crystal. While the definitions and general properties are rather abstract and **mathematical**, they can be quite relevant for theoretical studies of real three-dimensional crystals. As an example, lattice representations of crystals are required as input to any electronic structure calculation for solid crystalline material. Further, the theoretical treatment of three-dimensional crystals serves as a foundation to study the surfaces of single crystals, as will be discussed in Chapters 4, 5, and 6.

### 2.1 Basic Definition

The basic definition of a perfect three-dimensional bulk crystal becomes quite clear by considering a simple example. Figure 2.2a shows a section of the cubic CsCl crystal, which is periodic in three perpendicular directions. Thus, its periodicity can be described by orthogonal vectors  $\underline{R}_1$ ,  $\underline{R}_2$ ,  $\underline{R}_3$  (**lattice vectors**), as indicated in Figure 2.2b, whose lengths define the corresponding periodicity lengths. The lattice vectors span a cubic cell (**morphological unit cell**) that contains one cesium and one chlorine atom each at positions given by vectors  $\underline{r}_1$  (Cs) and  $\underline{r}_2$  (Cl) (**lattice basis vectors**), see Figure 2.2b. A periodic repetition

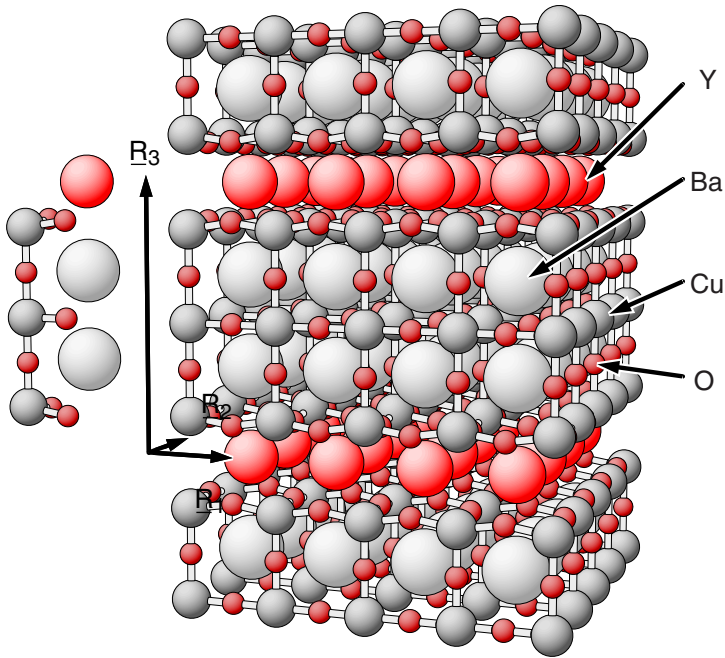


**Figure 2.1** Section of a tetragonal  $\text{YBa}_2\text{Cu}_3\text{O}_7$  crystal. The atoms are labeled accordingly. In addition, the basis of 13 atoms inside a rectangular cell and lattice vectors  $\underline{R}_1, \underline{R}_2, \underline{R}_3$  are included to the left.

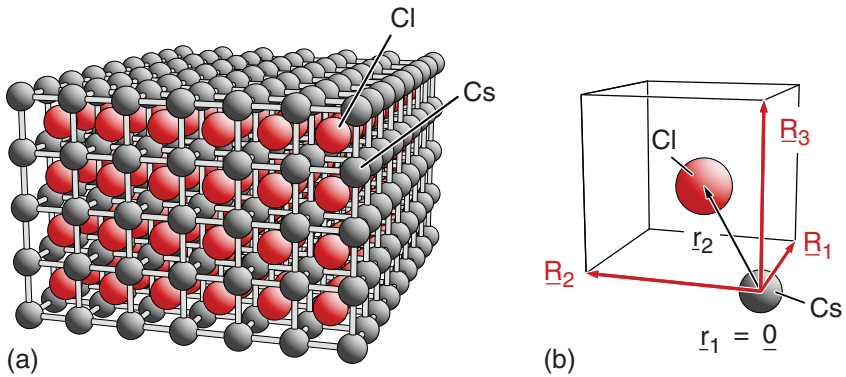


**Figure 2.2** (a) Section of a cubic  $\text{CsCl}$  crystal. Sticks connect neighboring Cs atoms to indicate the crystal structure. (b) Primitive morphological unit cell with two atoms, Cs and Cl, inside. The lattice vectors  $\underline{R}_1, \underline{R}_2, \underline{R}_3$  as well as lattice basis vectors,  $\underline{r}_1 = \underline{0}$  for Cs and  $\underline{r}_2$  for Cl, are shown and labeled accordingly.

of the unit cell along  $\underline{R}_1$ ,  $\underline{R}_2$ ,  $\underline{R}_3$  can then be used to build the complete infinite crystal.

In the general case, the formal definition of a perfect three-dimensional bulk **crystal** starts from a three-dimensionally periodic arrangement of atoms. Here, the crystal periodicity is described by a **lattice** with **lattice vectors**  $\underline{R}_1$ ,  $\underline{R}_2$ ,  $\underline{R}_3$ . Thus, the lattice forms an infinite and periodic array of **lattice points** reached from a common origin by vectors  $\underline{R}$  with

$$\underline{R} = n_1 \underline{R}_1 + n_2 \underline{R}_2 + n_3 \underline{R}_3 \quad (2.1)$$

where the coefficients  $n_1$ ,  $n_2$ ,  $n_3$  can assume any integer value. This means, in particular, that each lattice point experiences the same environment created by all other points.

The lattice vectors can be given in different ways, where the choice depends on the type of application. While for numerical calculations it may be preferable to define  $\underline{R}_1$ ,  $\underline{R}_2$ ,  $\underline{R}_3$  with respect to an absolute **Cartesian coordinate system** as

$$\underline{R}_i = (x_i, y_i, z_i), \quad i = 1, 2, 3 \quad (2.2)$$

it is common in the crystallographic literature to define these vectors by **lattice parameters** describing their lengths (**lattice constants**)  $a$ ,  $b$ ,  $c$  and by their mutual **angles**  $\alpha$ ,  $\beta$ ,  $\gamma$ , as sketched in Figure 2.3, where

$$a = |\underline{R}_1|, \quad b = |\underline{R}_2|, \quad c = |\underline{R}_3|$$

$$(\underline{R}_1 \underline{R}_2) = ab \cos(\gamma), \quad (\underline{R}_1 \underline{R}_3) = ac \cos(\beta), \quad (\underline{R}_2 \underline{R}_3) = bc \cos(\alpha) \quad (2.3)$$

Examples are given by lattices denoted as

$$\text{simple cubic} \quad \text{where} \quad a = b = c, \quad \alpha = \beta = \gamma = 90^\circ \quad (2.4)$$

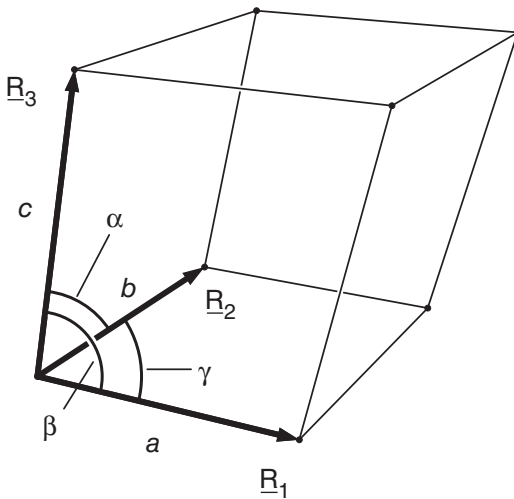


**Figure 2.3** Definition of crystallographic lattice parameters  $a$ ,  $b$ ,  $c$ ,  $\alpha$ ,  $\beta$ ,  $\gamma$  in a perspective view.

$$\text{hexagonal} \quad \text{where } a = b \neq c, \quad \alpha = \beta = 90^\circ, \gamma = 120^\circ \quad (2.5)$$

Relations (2.3) can be **converted** to yield lattice vectors in Cartesian coordinates starting from the six parameters,  $a$ ,  $b$ ,  $c$ , and  $\alpha$ ,  $\beta$ ,  $\gamma$ , given in Eq. (2.3), where one possible conversion is

$$\begin{aligned} \underline{R}_1 &= a(1, 0, 0), \quad \underline{R}_2 = b(\cos(\gamma), \sin(\gamma), 0) \\ \underline{R}_3 &= c(\cos(\beta), (\cos(\alpha) - \cos(\beta)\cos(\gamma))/\sin(\gamma), v_3/\sin(\gamma)) \end{aligned} \quad (2.6a)$$

with

$$v_3 = \{(\cos(\beta - \gamma) - \cos(\alpha))(\cos(\alpha) - \cos(\beta + \gamma))\}^{1/2} \quad (2.6b)$$

This yields for simple cubic (sc) lattices with Eq. (2.4)

$$\underline{R}_1 = a(1, 0, 0), \quad \underline{R}_2 = a(0, 1, 0), \quad \underline{R}_3 = a(0, 0, 1) \quad (2.7)$$

and for hexagonal lattices with Eq. (2.5)

$$\underline{R}_1 = a(1, 0, 0), \quad \underline{R}_2 = a(-1/2, \sqrt{3}/2, 0), \quad \underline{R}_3 = c(0, 0, 1) \quad (2.8)$$

The lattice vectors  $\underline{R}_1$ ,  $\underline{R}_2$ ,  $\underline{R}_3$  span a six-faced polyhedron (so-called parallelepiped), defining the **morphological unit cell**, often referred to as the **unit cell**, whose edges are parallel to  $\underline{R}_1$ ,  $\underline{R}_2$ ,  $\underline{R}_3$  and whose volume  $V_{\text{el}}$  is given by

$$V_{\text{el}} = |(\underline{R}_1 \times \underline{R}_2) \cdot \underline{R}_3| \quad (2.9)$$

The unit cell is called a **primitive unit cell** if its volume is the smallest of all possible unit cells in the crystal. This is equivalent to requiring that there is no additional lattice point, described by vector  $\underline{R}'$  with

$$\underline{R}' = \kappa_1 \underline{R}_1 + \kappa_2 \underline{R}_2 + \kappa_3 \underline{R}_3, \quad 0 \leq \kappa_i < 1 \quad (2.10)$$

inside the morphological unit cell of the lattice. Otherwise, the cell is **non-primitive** and there must be one or more additional lattice points  $\underline{R}'$  inside the unit cell. Analogously, lattice vectors  $\underline{R}_1$ ,  $\underline{R}_2$ ,  $\underline{R}_3$  whose morphological unit cell is primitive are called **primitive lattice vectors**, otherwise **non-primitive**. As an example, the cubic unit cell of CsCl as well as the corresponding lattice vectors, shown in Figure 2.2, are primitive. On the other hand, replacing all cesium and chlorine atoms in Figure 2.2 by one atom type, for example, iron, yields a body-centered cubic (bcc) crystal. Here, the lattice vectors  $\underline{R}_1$ ,  $\underline{R}_2$ ,  $\underline{R}_3$ , shown in the figure, are non-primitive, since vector  $\underline{r}_2$  now becomes a lattice vector inside the morphological unit cell.

In a crystal, the morphological unit cell contains, in general,  $p$  atoms at positions given by vectors  $\underline{r}_1, \dots, \underline{r}_p$  (**lattice basis vectors**), which form the **basis** of the crystal structure (the basis is sometimes also called the **structure**). Each atom at  $\underline{r}_i$  carries a **label** characterizing its properties, such as its nuclear charge or element name. These labels, usually omitted in the following, will be attached to each lattice basis vector if needed. For example, a definition  $\underline{r}_3^{\text{Cl}}$  would refer to a chlorine atom

placed at a position given by the third lattice basis vector. All lattice basis vectors  $\underline{r}_i$  inside the morphological unit cell can be written as **linear combinations** of the lattice vectors  $\underline{R}_1, \underline{R}_2, \underline{R}_3$  according to

$$\underline{r}_i = x_i \underline{R}_1 + y_i \underline{R}_2 + z_i \underline{R}_3, \quad i = 1 \dots p \quad (2.11)$$

where  $x_i, y_i,$  and  $z_i$  are real-valued coefficients with  $|x_i| < 1, |y_i| < 1, |z_i| < 1$ . This use of **relative coordinates**  $x_i, y_i, z_i$  to describe atoms inside the unit cell is common practice in the crystallographic literature [28–33]. Note that, according to definition (2.11) the coefficients  $x_i, y_i, z_i$  are generally not connected with the Cartesian coordinate system but with coordinate axes given by the lattice vectors  $\underline{R}_1, \underline{R}_2, \underline{R}_3$ .

The **origin** of the morphological unit cell inside a crystal can always be chosen freely since the complete infinite crystal consists of a periodic arrangement of unit cells in three dimensions. In particular, the origin does not need to coincide with a specific atom position, as considered in the example of CsCl discussed above. However, it is usually chosen to coincide with the location of the largest number of point symmetry elements, such as inversion points or origins of mirror planes and rotation axes, which are given by the lattice vectors  $\underline{R}_1, \underline{R}_2, \underline{R}_3$  together with the lattice basis vectors  $\underline{r}_1, \dots, \underline{r}_p$ . This will be discussed in greater detail in Section 2.4.

Altogether, a **crystal** is characterized uniquely by its **lattice** defined by lattice vectors  $\underline{R}_1, \underline{R}_2, \underline{R}_3$  and its **basis** defined by lattice basis vectors  $\underline{r}_1, \dots, \underline{r}_p$ . Thus, general atom positions inside the crystal can be given by

$$\underline{r} = n_1 \underline{R}_1 + n_2 \underline{R}_2 + n_3 \underline{R}_3 + \underline{r}_i \quad (2.12)$$

where the coefficients  $n_1, n_2, n_3$  can assume any integer value and index  $i = 1, \dots, p$  counts the number of atoms in the unit cell. Here, the lattice and the basis can be treated as **separate** elements of a crystal structure (which are only connected by the symmetry elements as will be discussed in Section 2.4).

## 2.2

### Representation of Bulk Crystals

There is one important aspect that characterizes all formal descriptions of crystal structures, the fact that mathematical descriptions of crystals are **not unique**. This means that, for a given definition of a crystal, one can always find an infinite number of alternatives that describe the same crystal. While this ambiguity may be considered a drawback at first glance, it allows choosing crystal representations according to additional constraints, for example, those given by symmetry, physical, or chemical properties. Here, one can distinguish between alternative descriptions that affect the crystal basis but not its lattice representation and those where both the lattice representation and the basis are affected.

## 2.2.1

**Alternative Descriptions Conserving the Lattice Representation**

Examples of alternative crystal descriptions that do not affect the crystal lattice are given by elemental or compound **decompositions** of a crystal. Here, the basic idea is to decompose the basis inside the unit cell of a complex crystal into components and consider (fictitious) crystals of these components with the same periodicity as that of the initial crystal, given by its lattice. This decomposition is of didactic value but may also help to understand details of chemical binding inside the crystal, for example, discriminating between intra- and inter-molecular binding in molecular crystals. In the simplest case, a crystal with  $p$  atoms in its primitive unit cell can be considered alternatively as a combination of  $p$  crystals with the same lattice but with only one atom in their primitive unit cells. The origins of the corresponding  $p$  crystals can be set at positions given by the lattice basis vectors  $\underline{r}_i$  of the complete non-primitive crystal.

As a very simple example, the cubic **cesium chloride**, CsCl, crystal, shown in Figure 2.2, is defined by a simple cubic (sc) lattice with lattice vectors  $\underline{R}_1, \underline{R}_2, \underline{R}_3$  given by Eq. (2.7). Further, its basis includes two atoms, Cs and Cl, which can be positioned at

$$\underline{r}_1 = a(0, 0, 0) \text{ for Cs, } \underline{r}_2 = a(1/2, 1/2, 1/2) \text{ for Cl} \quad (2.13)$$

with  $a$  denoting the lattice constant of CsCl. Thus, the crystal can be considered as a combination of two sc monoatomic crystals, one for cesium and one for chlorine, where their origins are shifted by  $\underline{r}_o = \underline{r}_2 - \underline{r}_1 = a(1/2, 1/2, 1/2)$  with respect to each other.

A more complex example is the tetragonal **YBa<sub>2</sub>Cu<sub>3</sub>O<sub>7</sub>** crystal, shown in Figure 2.1. Here, the lattice vectors can be written in Cartesian coordinates as

$$\underline{R}_1 = a(1, 0, 0), \quad \underline{R}_2 = a(0, 1, 0), \quad \underline{R}_3 = c(0, 0, 1) \quad (2.14a)$$

and the morphological unit cell contains 13 atoms resulting in 13 lattice basis vectors  $\underline{r}_i$  with

$$\begin{aligned} \text{Y atom :} & \quad \underline{r}_1 = (1/2, 1/2, 5/6) \\ \text{Ba atoms :} & \quad \underline{r}_2 = (1/2, 1/2, 1/6), \quad \underline{r}_3 = (1/2, 1/2, 1/2) \\ \text{Cu atoms :} & \quad \underline{r}_4 = (0, 0, 0), \quad \underline{r}_5 = (0, 0, 1/3), \quad \underline{r}_6 = (0, 0, 2/3) \\ \text{O atoms :} & \quad \underline{r}_7 = (1/2, 0, -\varepsilon), \quad \underline{r}_8 = (0, 1/2, -\varepsilon), \quad \underline{r}_9 = (0, 0, 1/6) \\ & \quad \underline{r}_{10} = (0, 1/2, 1/3), \quad \underline{r}_{11} = (0, 0, 1/2) \\ & \quad \underline{r}_{12} = (1/2, 0, 2/3 + \varepsilon), \quad \underline{r}_{13} = (0, 1/2, 2/3 + \varepsilon) \end{aligned} \quad (2.14b)$$

using relative coordinates (2.11) where experiments yield a relative position shift  $\varepsilon = 0.026$  of four oxygen atoms. This crystal can be decomposed conceptually into 13 monoatomic (tetragonal) crystals, one yttrium, two barium, three copper, and seven oxygen crystals.

Alternatively, one can decompose the YBa<sub>2</sub>Cu<sub>3</sub>O<sub>7</sub> crystal into physically more meaningful subunits that include **several** of the atoms of the initial unit cell. As an

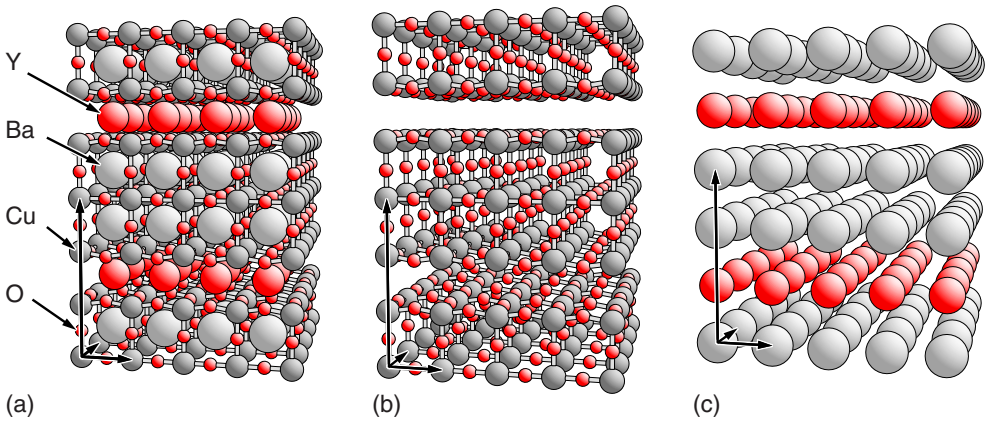


**Figure 2.4** Decomposition of the  $\text{YBa}_2\text{Cu}_3\text{O}_7$  crystal (a) into its copper oxide,  $\text{Cu}_3\text{O}_7$  (b) and heavy metal,  $\text{YBa}_2$ , components (c). Atoms are shown as colored balls and labeled accordingly. In addition, the lattice vectors  $\underline{R}_1$ ,  $\underline{R}_2$ ,  $\underline{R}_3$  are indicated by arrows.

example, Figure 2.4 illustrates a decomposition of the  $\text{YBa}_2\text{Cu}_3\text{O}_7$  crystal into its copper oxide and its heavy metal components, namely,  $\text{Cu}_3\text{O}_7$  and  $\text{YBa}_2$ , respectively. Here, the unit cells of the component crystals contain 10 and 3 atoms each, where the  $\text{Cu}_3\text{O}_7$  component is believed to contribute to the high-temperature superconductivity of  $\text{YBa}_2\text{Cu}_3\text{O}_7$ .

A very illustrative example of crystal decomposition is given by the **diamond** crystal, shown in Figure 2.5. Its lattice can be defined as a cubic lattice where the lattice vectors are given by Eq. (2.7). The basis of the crystal includes eight carbon atoms in tetrahedral arrangements resulting in eight lattice basis vectors  $\underline{r}_i$  with

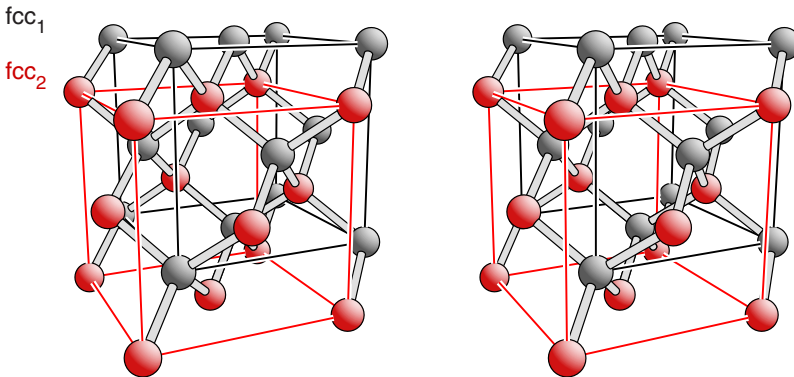


**Figure 2.5** Decomposition of the diamond crystal into two (shifted) face-centered cubic crystals, denoted  $\text{fcc}_1$  (gray balls, black lines) and  $\text{fcc}_2$  (red balls and red lines). The crystal is shown in a stereo view where the visual three-dimensional impression is obtained by cross-eyed viewing.

$$\begin{aligned}
\underline{r}_1 &= (0, 0, 0), & \underline{r}_2 &= (0, 1/2, 1/2), & \underline{r}_3 &= (1/2, 0, 1/2) \\
\underline{r}_4 &= (1/2, 1/2, 0), & \underline{r}_5 &= (1/4, 1/4, 1/4), & \underline{r}_6 &= (1/4, 3/4, 3/4) \\
\underline{r}_7 &= (3/4, 1/4, 3/4), & \underline{r}_8 &= (3/4, 3/4, 1/4)
\end{aligned} \tag{2.15}$$

in relative coordinates (2.11). This shows, first, that the diamond crystal can be decomposed into eight sc crystals, each with one carbon in the primitive unit cell. Further, the lattice basis vectors  $\underline{r}_5, \underline{r}_6, \underline{r}_7, \underline{r}_8$  arise from  $\underline{r}_1, \underline{r}_2, \underline{r}_3, \underline{r}_4$  by identical shifts with

$$\underline{r}_{i+4} = \underline{r}_i + 1/4 (1, 1, 1), \quad i = 1, 2, 3, 4 \tag{2.16}$$

This suggests that the diamond crystal can also be decomposed into two identical cubic crystals, each with four atoms in their unit cells, where the origins of the two crystals are shifted by a vector  $a/4 (1, 1, 1)$  with respect to each other. The lattices of the two component crystals will be shown in Section 2.2.2.1 to be identical to face-centered cubic (fcc) lattices. Thus, the diamond crystal can be alternatively described by a superposition of two fcc crystals which becomes clear by an inspection of Figure 2.5.

## 2.2.2

### Alternative Descriptions Affecting the Lattice Representation

There are many possibilities of providing alternative descriptions of crystals where their lattices are represented differently. These alternatives may be preferred because of **conceptual** convenience but may also be required due to **computational** necessity. Examples are symmetry-adapted lattices combining translational with point symmetry properties or surface-adapted lattices facilitating the definition of atom coordinates in surface studies.

Crystallographers have defined a set of constraints on lattice vectors  $\underline{R}_1, \underline{R}_2, \underline{R}_3$  to yield a unique description of a lattice according to Niggli [41], which allows an easy distinction between the different types of three-dimensional Bravais lattices discussed in Section 2.4. First, the lattice vectors are chosen such that they form a right-handed vector triplet, which can be expressed mathematically by the constraint

$$(\underline{R}_1 \times \underline{R}_2) \cdot \underline{R}_3 > 0 \tag{2.17}$$

Further, they are assumed to reflect three smallest periodicity lengths along different directions in the crystal and are arranged such that

$$|\underline{R}_1| \leq |\underline{R}_2| \leq |\underline{R}_3| \tag{2.18}$$

In addition, all lattices are grouped according to their scalar products  $s_{ij} = (\underline{R}_i \cdot \underline{R}_j)$  into two classes,

$$s_{12} \geq 0, \quad s_{13} \geq 0, \quad s_{23} \geq 0 \quad (\text{type 1, acute}) \tag{2.19a}$$

$$s_{12} \leq 0, \quad s_{13} \leq 0, \quad s_{23} \leq 0, \quad \text{with at least one } s_{ij} < 0 \quad (\text{type 2, obtuse}) \tag{2.19b}$$

where lattices with other  $s_{ij}$  combinations can be easily converted to one of the two classes by inverting two of the lattice vectors  $\underline{R}_i, \underline{R}_j$  to yield  $-\underline{R}_i, -\underline{R}_j$ . Further, simple iterative algorithms have been developed [42, 43] to reduce a general vector set  $\underline{R}_1, \underline{R}_2, \underline{R}_3$  of type 1 or 2 to a unique description with  $\underline{R}_1, \underline{R}_2, \underline{R}_3$  referring to vectors of smallest length in the lattice. This **reduced lattice vector set** fulfills, apart from Eqs. (2.17) and (2.18), the inequalities

$$-\min(\underline{R}_i^2, \underline{R}_j^2) \leq 2(\underline{R}_i \underline{R}_j) < \min(\underline{R}_i^2, \underline{R}_j^2), \quad i \neq j, \quad i, j = 1, 2, 3 \quad (2.20)$$

which can be used to identify and classify reduced unique vector sets  $\underline{R}_1, \underline{R}_2, \underline{R}_3$ . Type 2 lattices require an additional constraint which reads

$$2(|\underline{R}_1 \underline{R}_2| + |\underline{R}_1 \underline{R}_3| + |\underline{R}_2 \underline{R}_3|) \leq \underline{R}_1^2 + \underline{R}_2^2 \quad (2.21)$$

to yield a unique description [42].

The application of the above constraints to two-dimensional lattices described by lattice vectors  $\underline{R}_1, \underline{R}_2$  is straightforward. Here, the two vectors are required to yield the smallest periodicity lengths along different directions in the lattice and are ordered according to

$$|\underline{R}_1| \leq |\underline{R}_2| \quad (2.22)$$

This allows, as in the three-dimensional case, two lattice classes differing by the scalar product  $s_{12} = (\underline{R}_1 \underline{R}_2)$ ,

$$s_{12} \geq 0 \quad (\text{type 1, **acute**}) \quad \text{and} \quad s_{12} < 0 \quad (\text{type 2, **obtuse**}) \quad (2.23)$$

The Minkowski reduction, see Section 3.3 and Appendix D, can be used to reduce a general vector set  $\underline{R}_1, \underline{R}_2$  of type 1 or 2 to a unique description referring to vectors of smallest length in the lattice. This reduced vector set fulfills, apart from Eq. (2.22), the inequality

$$-\min(\underline{R}_1^2, \underline{R}_2^2) \leq 2(\underline{R}_1 \underline{R}_2) < \min(\underline{R}_1^2, \underline{R}_2^2) \quad (2.24)$$

which can be used to test whether a vector set  $\underline{R}_1, \underline{R}_2$  is reduced or not. The constraints (2.22) and (2.24) yield a unique description that allows a simple distinction between the different types of two-dimensional Bravais lattices discussed in Section 3.7. They can also serve as a basis for a more general classification scheme proposed in the literature [44]. In two dimensions, obtuse lattice descriptions can always be converted to acute descriptions, which is preferred by many surface scientists, by swapping the lattice vectors and replacing one of the two, for example,  $\underline{R}_1$ , by its negative,  $-\underline{R}_1$ , where, however, one of the two representations may violate constraint (2.22).

Many researchers in the surface science community (and not only there) find it convenient to think in Cartesian coordinates, using orthogonal unit vectors in three-dimensional space. Therefore, they prefer to characterize lattices, if possible, by orthogonal lattice vectors  $\underline{R}_1, \underline{R}_2, \underline{R}_3$  even at the expense of having to consider corresponding crystal bases with a larger number of atoms. This will be discussed for face- and body-centered cubic lattices in Section 2.2.2.1.

Theoretical studies on extended geometric perturbations inside a crystal, such as those originating from periodic imperfections or distortions, often require considering unit cells with lattice vectors  $\underline{R}'_1, \underline{R}'_2, \underline{R}'_3$  which are larger than those given by  $\underline{R}_1, \underline{R}_2, \underline{R}_3$  of the unperturbed crystal. Here, a direct computational comparison of results for the perturbed crystal with those for the unperturbed crystal is often facilitated by applying the same (enlarged) lattice vectors  $\underline{R}'_1, \underline{R}'_2, \underline{R}'_3$  to both systems. As a result, the unperturbed crystal is described by a lattice with a larger than primitive unit cell and an appropriately increased number of atoms. This is the basic idea behind so-called **superlattice** methods, which will be discussed in Section 2.2.2.2.

Ideal single crystal surfaces that originate from bulk truncation yielding two-dimensional periodicity at the surface, will be treated in great detail in Chapter 4. Here, the analysis of structural properties at the surface can be facilitated greatly by using so-called **netplane-adapted** lattice vectors  $\underline{R}'_1, \underline{R}'_2, \underline{R}'_3$ . These are given by linear transformations of the initial bulk lattice vectors, where the shape of the morphological unit cell may change but not its volume nor the number of atoms inside the cell. Differently oriented surfaces require different sets of netplane-adapted lattice vectors leading to many alternative descriptions of the bulk lattice, as discussed in Section 2.2.2.3.

### 2.2.2.1 Cubic, Hexagonal, and Trigonal Lattices

The family of cubic lattices, simple, body-, and face-centered, are closely connected with each other, which is why many scientists use the simplest of the three, the simple cubic lattice as their reference. This lattice, also called **cubic-P** and often abbreviated by **sc** is described in Cartesian coordinates by lattice vectors

$$\underline{R}_1^{\text{sc}} = a(1, 0, 0), \quad \underline{R}_2^{\text{sc}} = a(0, 1, 0), \quad \underline{R}_3^{\text{sc}} = a(0, 0, 1) \quad (2.25)$$

which are three mutually orthogonal vectors of equal length, given by the lattice constant  $a$ .

The **body-centered cubic** lattice, also called **I-centered** or **cubic-I** and often abbreviated by **bcc**, see Figure 2.6, can be defined in Cartesian coordinates by lattice vectors

$$\underline{R}_1 = a/2(-1, 1, 1), \quad \underline{R}_2 = a/2(1, -1, 1), \quad \underline{R}_3 = a/2(1, 1, -1) \quad (2.26)$$

Here, the three vectors are of the same length

$$|\underline{R}_1| = |\underline{R}_2| = |\underline{R}_3| = (\sqrt{3}/2)a \quad (2.27)$$

but they are not orthogonal to each other, forming angles  $\alpha = \beta = \gamma = 109.47^\circ$  ( $\cos \alpha = -1/3$ ) according to Eq. (2.3). **General lattice points** of the bcc lattice are given in Cartesian coordinates by vectors

$$\begin{aligned} \underline{R} &= n_1 \underline{R}_1 + n_2 \underline{R}_2 + n_3 \underline{R}_3 \\ &= a/2(-n_1 + n_2 + n_3, n_1 - n_2 + n_3, n_1 + n_2 - n_3) \\ &= a/2(N_1, N_2, N_3), \quad n_1, n_2, n_3, N_1, N_2, N_3 \text{ integer} \end{aligned} \quad (2.28)$$

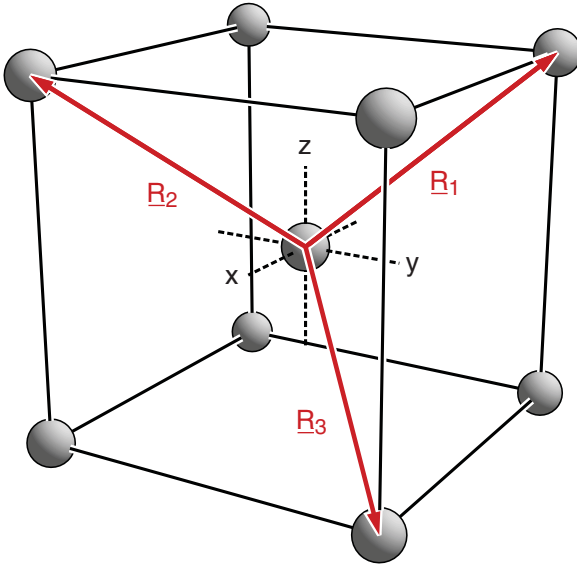


**Figure 2.6** Lattice vectors  $\underline{R}_1$ ,  $\underline{R}_2$ ,  $\underline{R}_3$  of the body-centered cubic (bcc) lattice sketched inside a cubic frame with Cartesian coordinates,  $x$ ,  $y$ , and  $z$ , indicated. Atoms of the corresponding bcc crystal are shown as balls.

where the integers  $n_1, n_2, n_3$  and  $N_1, N_2, N_3$  are connected by

$$N_1 = -n_1 + n_2 + n_3, \quad N_2 = n_1 - n_2 + n_3, \quad N_3 = n_1 + n_2 - n_3 \quad (2.29)$$

Relation (2.28) together with the definition of the sc lattice vectors can be written as

$$\underline{R} = n_1 \underline{R}_1 + n_2 \underline{R}_2 + n_3 \underline{R}_3 = 1/2 (N_1 \underline{R}_1^{\text{sc}} + N_2 \underline{R}_2^{\text{sc}} + N_3 \underline{R}_3^{\text{sc}}) \quad (2.30)$$

which demonstrates the connection between the bcc and the sc lattices. While the integer coefficients  $n_1, n_2, n_3$  can be chosen freely the integer coefficients  $N_1, N_2, N_3$  are not independent. Relations (2.29) yield

$$N_2 = N_1 + 2(n_1 - n_2), \quad N_3 = N_1 + 2(n_1 - n_3) \quad (2.31)$$

Hence, the integers  $N_1, N_2, N_3$  can only be all odd or all even for any choice of  $n_1, n_2, n_3$ .

If  $N_1, N_2, N_3$  in Eq. (2.28) are **all even**, that is, they can be represented by

$$N_i = 2m_i, \quad i = 1, 2, 3 \quad \text{for any integer } m_i \quad (2.32)$$

then relation (2.30) together with Eq. (2.32) leads to

$$\underline{R} = m_1 \underline{R}_1^{\text{sc}} + m_2 \underline{R}_2^{\text{sc}} + m_3 \underline{R}_3^{\text{sc}} \quad m_1, m_2, m_3 \text{ integer} \quad (2.33)$$

which describes an sc lattice as one subset of the bcc lattice.

If, on the other hand,  $N_1, N_2, N_3$  in Eq. (2.28) are **all odd**, that is, they can be represented by

$$N_i = 2m_i + 1, \quad i = 1, 2, 3 \quad \text{for any integer } m_i \quad (2.34)$$

then relation (2.30) together with Eq. (2.34) leads to

$$\underline{R} = m_1 \underline{R}_1^{\text{sc}} + m_2 \underline{R}_2^{\text{sc}} + m_3 \underline{R}_3^{\text{sc}} + \underline{v} \quad m_1, m_2, m_3 \text{ integer} \quad (2.35)$$

with

$$\underline{v} = 1/2 (\underline{R}_1^{\text{sc}} + \underline{R}_2^{\text{sc}} + \underline{R}_3^{\text{sc}}) \quad (2.36)$$

This also describes an sc lattice as the second subset of the bcc lattice, where the second sc lattice is, however, shifted by a vector  $\underline{v}$  with respect to the first. Thus, the constraints for  $N_1, N_2, N_3$  in Eq. (2.29) yield a decomposition of the bcc lattice into **two** identical sc lattices that are shifted with respect to each other by vector  $\underline{v}$  given by Eq. (2.36). The two sc lattices are sketched in Figure 2.7 and denoted “ $sc_1$ ”, “ $sc_2$ ” in the figure.

As a consequence, any crystal with a bcc lattice given by lattice vectors (2.26) can be alternatively described by a crystal with an sc lattice with lattice vectors (2.25), where the unit cell of the sc lattice contains twice as many atoms with atom pairs separated by vector  $\underline{v}$ . Further, the lattice vectors  $\underline{R}_1^{\text{sc}}, \underline{R}_2^{\text{sc}}, \underline{R}_3^{\text{sc}}$  of the sc lattice representation are **non-primitive** since vector

$$\underline{v} = 1/2 (\underline{R}_1^{\text{sc}} + \underline{R}_2^{\text{sc}} + \underline{R}_3^{\text{sc}}) = \underline{R}_1 + \underline{R}_2 + \underline{R}_3 \quad (2.37)$$

according to Eq. (2.26) is a true lattice vector.

The **face-centered cubic** lattice, also called **F-centered** or **cubic-F** and often abbreviated by **fcc**, see Figure 2.8, can be defined in Cartesian coordinates by lattice vectors

$$\underline{R}_1 = a/2 (0, 1, 1), \quad \underline{R}_2 = a/2 (1, 0, 1), \quad \underline{R}_3 = a/2 (1, 1, 0) \quad (2.38)$$

As for the bcc lattice, the three vectors are of the same length

$$|\underline{R}_1| = |\underline{R}_2| = |\underline{R}_3| = a/\sqrt{2} \quad (2.39)$$

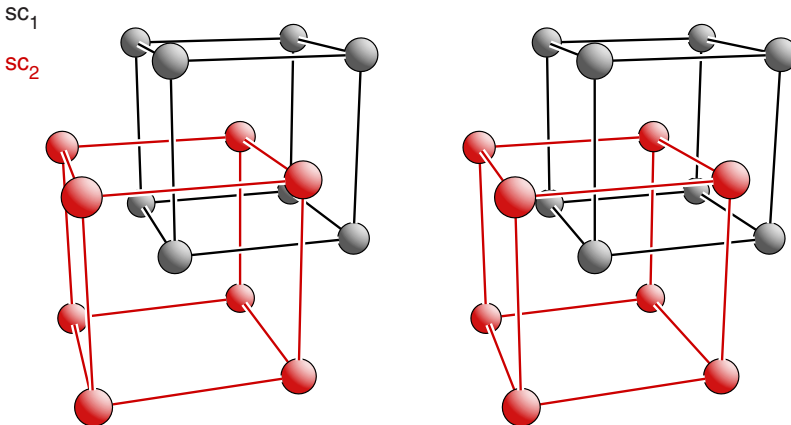


**Figure 2.7** Visual decomposition of the bcc crystal into two (shifted) sc crystals, denoted  $sc_1$  (gray balls, black lines) and  $sc_2$  (red balls and lines). The crystal is shown in a stereo view where the visual three-dimensional impression is obtained by cross-eyed viewing.

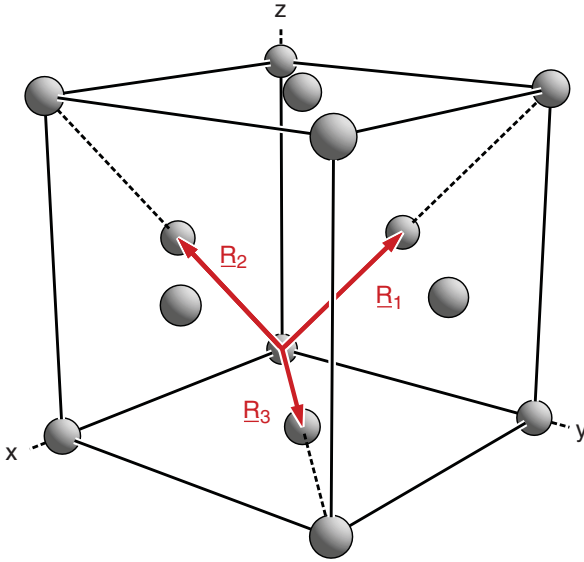


**Figure 2.8** Lattice vectors  $\underline{R}_1$ ,  $\underline{R}_2$ ,  $\underline{R}_3$  of the fcc lattice sketched inside a cubic frame and labeled accordingly. Atoms of the corresponding fcc crystal are shown as balls. The dashed lines are meant to assist the visual orientation inside the figure.

but are not orthogonal to each other, forming angles  $\alpha = \beta = \gamma = 60^\circ$  ( $\cos \alpha = 1/2$ ) according to Eq. (2.3). **General lattice points** of the fcc lattice are given in Cartesian coordinates by vectors

$$\begin{aligned} \underline{R} &= n_1 \underline{R}_1 + n_2 \underline{R}_2 + n_3 \underline{R}_3 = a/2 (n_2 + n_3, n_1 + n_3, n_1 + n_2) \\ &= a/2 (N_1, N_2, N_3), \quad n_1, n_2, n_3, N_1, N_2, N_3 \text{ integer} \end{aligned} \quad (2.40)$$

where the integers  $n_1$ ,  $n_2$ ,  $n_3$  and  $N_1$ ,  $N_2$ ,  $N_3$  are connected by

$$N_1 = n_2 + n_3, \quad N_2 = n_1 + n_3, \quad N_3 = n_1 + n_2 \quad (2.41)$$

Relation (2.40) together with the definition of the sc lattice vectors can be written as

$$\underline{R} = n_1 \underline{R}_1 + n_2 \underline{R}_2 + n_3 \underline{R}_3 = 1/2 (N_1 \underline{R}_1^{\text{sc}} + N_2 \underline{R}_2^{\text{sc}} + N_3 \underline{R}_3^{\text{sc}}) \quad (2.42)$$

which shows the connection between the fcc and the sc lattice. As in the bcc case, the integer coefficients  $N_1$ ,  $N_2$ ,  $N_3$  are not independent. Even- and odd-valued combinations of the initial coefficients  $n_1$ ,  $n_2$ ,  $n_3$  yield eight cases as shown in Table 2.1.

As a result, integers  $N_1$ ,  $N_2$ ,  $N_3$  reduce to **four** different types of **even/odd combinations**,

- 1)  $N_i = 2m_i$ ,  $i = 1, 2, 3$ , (cases 1, 2 in Table 2.1) which results, according to Eq. (2.42), in

$$\underline{R} = a/2 (N_1, N_2, N_3) = a (m_1, m_2, m_3), \quad m_1, m_2, m_3 \text{ integer} \quad (2.43a)$$

**Table 2.1** List of all possible even/odd integer combinations  $N_1, N_2, N_3$  following from even/odd integer combinations  $n_1, n_2, n_3$  according to Eq. (2.41).

Case	$n_1$	$n_2$	$n_3$	$N_1$	$N_2$	$N_3$
1	e	e	e	e	e	e
2	o	o	o	e	e	e
3	o	e	e	e	o	o
4	e	o	o	e	o	o
5	e	o	e	o	e	o
6	o	e	o	o	e	o
7	e	e	o	o	o	e
8	o	o	e	o	o	e

Characters “e” and “o” stand for even and odd integers, respectively.

describing the sc lattice given by Eq. (2.25) with its origin coinciding with that of the fcc lattice, corresponding to an origin shift  $\underline{v}_1 = \underline{0}$ , see below.

- 2)  $N_1 = 2m_1, N_2 = 2m_2 + 1, N_3 = 2m_3 + 1$ , (cases 3, 4) resulting in

$$\begin{aligned}\underline{R} &= a/2 (N_1, N_2, N_3) = a (m_1, m_2, m_3) + \underline{v}_2 \\ \underline{v}_2 &= 1/2 (\underline{R}_2^{\text{sc}} + \underline{R}_3^{\text{sc}})\end{aligned}\quad (2.43b)$$

describing the sc lattice with an origin shift  $\underline{v}_2$ .

- 3)  $N_1 = 2m_1 + 1, N_2 = 2m_2, N_3 = 2m_3 + 1$ , (cases 5, 6) resulting in

$$\begin{aligned}\underline{R} &= a/2 (N_1, N_2, N_3) = a (m_1, m_2, m_3) + \underline{v}_3 \\ \underline{v}_3 &= 1/2 (\underline{R}_1^{\text{sc}} + \underline{R}_3^{\text{sc}})\end{aligned}\quad (2.43c)$$

describing the sc lattice with an origin shift  $\underline{v}_3$ .

- 4)  $N_1 = 2m_1 + 1, N_2 = 2m_2 + 1, N_3 = 2m_3$ , (cases 7, 8) resulting in

$$\begin{aligned}\underline{R} &= a/2 (N_1, N_2, N_3) = a (m_1, m_2, m_3) + \underline{v}_4 \\ \underline{v}_4 &= 1/2 (\underline{R}_1^{\text{sc}} + \underline{R}_2^{\text{sc}})\end{aligned}\quad (2.43d)$$

describing the sc lattice with an origin shift  $\underline{v}_4$ .

Therefore, the constraints for  $N_1, N_2, N_3$  in Eq. (2.41) yield a decomposition of the fcc lattice into **four** identical sc lattices that are shifted with respect to each other according to their origins at  $\underline{v}_1, \underline{v}_2, \underline{v}_3, \underline{v}_4$ , given by Eqs. (2.43a–2.43d). The four sc lattices are sketched in Figure 2.9 and denoted “ $\text{sc}_1$ ” to “ $\text{sc}_4$ ” in the figure.

As a consequence, any crystal with an fcc lattice given by lattice vectors Eq. (2.38) can be alternatively described by a crystal with an sc lattice with lattice vectors Eq. (2.25), where the unit cell of the sc lattice contains four times as many atoms with atom pairs separated by vectors  $\underline{v}_i - \underline{v}_j$ ,  $i, j = 1, \dots, 4$ . Further, the lattice vectors  $\underline{R}_1^{\text{sc}}, \underline{R}_2^{\text{sc}}, \underline{R}_3^{\text{sc}}$  of the sc lattice representation are **non-primitive** since

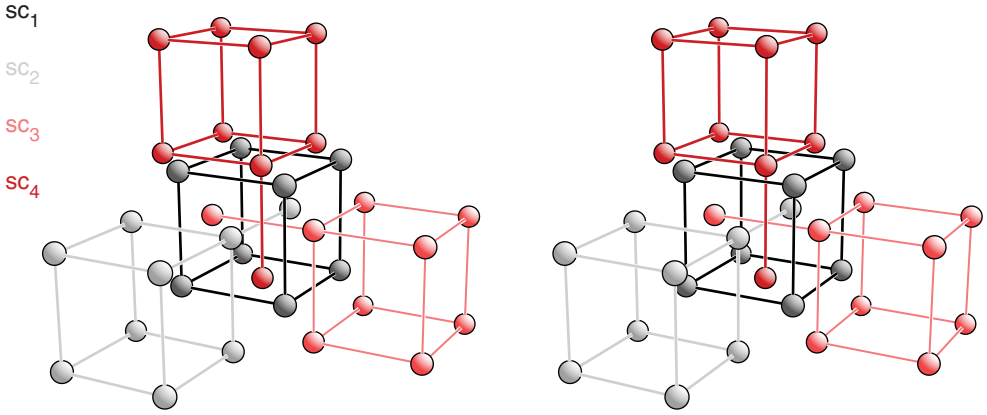


**Figure 2.9** Visual decomposition of the fcc crystal into four (shifted) sc crystals, denoted  $sc_1$  (dark gray balls, black lines),  $sc_2$  (dark red balls and lines),  $sc_3$  (light gray balls and lines), and  $sc_4$  (light red balls and lines). The crystal is shown in a stereo view where the visual three-dimensional impression is obtained by cross-eyed viewing.

the four vectors  $\underline{v}_i$

$$\begin{aligned} \underline{v}_1 &= \underline{0} & \underline{v}_2 &= 1/2 (\underline{R}_2^{sc} + \underline{R}_3^{sc}) = \underline{R}_1 \\ \underline{v}_3 &= 1/2 (\underline{R}_1^{sc} + \underline{R}_3^{sc}) = \underline{R}_2 & \underline{v}_4 &= 1/2 (\underline{R}_1^{sc} + \underline{R}_2^{sc}) = \underline{R}_3 \end{aligned} \quad (2.44)$$

according to Eq. (2.38) are true lattice vectors.

The **hexagonal** lattice, also called **hexagonal-P** and often abbreviated by **hex**, is described by two lattice vectors  $\underline{R}_1^{\text{hex}}$ ,  $\underline{R}_2^{\text{hex}}$  of equal length  $a$ , forming an angle of either  $120^\circ$  (**obtuse representation**) or  $60^\circ$  (**acute representation**) between them. A third lattice vector  $\underline{R}_3^{\text{hex}}$  of length  $c$ , is perpendicular to both  $\underline{R}_1^{\text{hex}}$  and  $\underline{R}_2^{\text{hex}}$ . Thus, the vectors of the obtuse representation can be described in Cartesian coordinates by

$$\underline{R}_1^{\text{hex}} = a(1, 0, 0), \quad \underline{R}_2^{\text{hex}} = a(-1/2, \sqrt{3}/2, 0), \quad \underline{R}_3^{\text{hex}} = c(0, 0, 1) \quad (2.45a)$$

and those of the acute representation by

$$\underline{R}_1^{\text{hex}} = a(1, 0, 0), \quad \underline{R}_2^{\text{hex}} = a(1/2, \sqrt{3}/2, 0), \quad \underline{R}_3^{\text{hex}} = c(0, 0, 1) \quad (2.45b)$$

where  $a$  and  $c$  are the lattice constants of the hexagonal lattice. While the two representations are equivalent, the **obtuse** representation of crystal lattices is often **preferred** over the acute one and will be used in the following discussions.

There is a special type of crystal structure with hexagonal lattice, the so-called **hexagonal close-packed (hcp)** crystal structure, illustrated by Figure 2.10 and called **hex (hcp)** in the following it is defined by a hexagonal lattice, given in obtuse representation by Eq. (2.45a) with a lattice constant ratio  $c/a$  of  $\sqrt{8/3} = 1.63299$ .

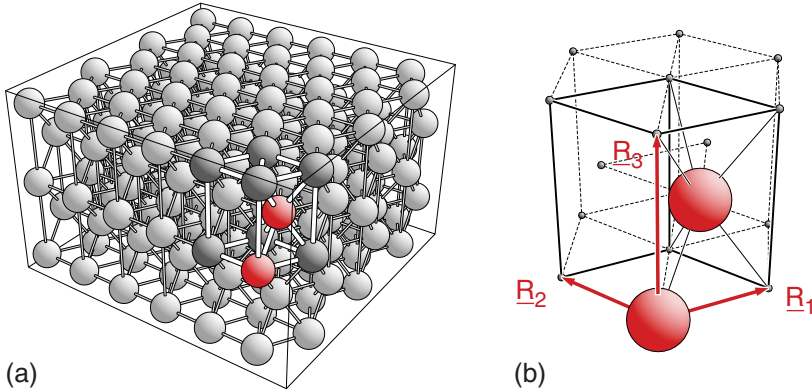


**Figure 2.10** (a) Section of a hexagonal crystal with close-packed geometry (hcp). Sticks connect atoms with nearest and second nearest neighbors to indicate the crystal structure. (b) Primitive morphological unit cell with two atoms inside. The lattice vectors  $\underline{R}_1$ ,  $\underline{R}_2$ ,  $\underline{R}_3$  (obtuse representation) are labeled accordingly. The unit cell is embedded in a hexagonal environment (dashed lines) to indicate its symmetry.

Further, the hexagonal unit cell contains two identical atoms at positions

$$\underline{r}_1^{\text{hcp}} = a(0, 0, 0), \quad \underline{r}_2^{\text{hcp}} = (a/2, a/\sqrt{12}, c/2) = a(1/2, 1/\sqrt{12}, \sqrt{2/3}) \quad (2.45c)$$

see Figure 2.10b. The  $c/a$  ratio and the atom positions are chosen such that each atom is surrounded by 12 nearest neighbor atoms at equal distance (equal to lattice constant  $a$ ), achieving the same atom density as crystals with a corresponding fcc lattice. While hcp crystals in their rigorous mathematical definition do not exist in nature, they occur, to a good approximation, that is, with ratios  $c/a$  close to  $\sqrt{8/3}$ , for many single crystals of metals, such as beryllium, magnesium, titanium, cobalt, ruthenium, and cadmium, see Table B.3.

Analogous to the family of cubic lattices, there is also a close connection between trigonal and hexagonal lattices, where scientists often prefer hexagonal over trigonal lattice descriptions. The **trigonal** lattice, also called **trigonal-R** or **rhombohedral**, is described by three lattice vectors  $\underline{R}_1$ ,  $\underline{R}_2$ ,  $\underline{R}_3$  of equal length  $a$ , which form identical angles  $\alpha = \beta = \gamma$ . Thus, the lattice vectors can be thought of as arising from each other by a  $120^\circ$  rotation about a common axis given by  $(\underline{R}_1 + \underline{R}_2 + \underline{R}_3)$ , see Figure 2.11a. Assuming the rotation axis as the  $z$  axis of a Cartesian coordinate system, the vectors can be described in Cartesian coordinates by

$$\begin{aligned} \underline{R}_1 &= a(c_1, 0, c_2), & \underline{R}_2 &= a(-1/2 c_1, \sqrt{3}/2 c_1, c_2), \\ \underline{R}_3 &= a(-1/2 c_1, -\sqrt{3}/2 c_1, c_2), & c_1 &= \cos(\varphi), \quad c_2 = \sin(\varphi) \end{aligned} \quad (2.46)$$

where  $\varphi$  denotes the angle between each of the three lattice vectors and the  $xy$  plane, see Figure 2.11a, and is determined by

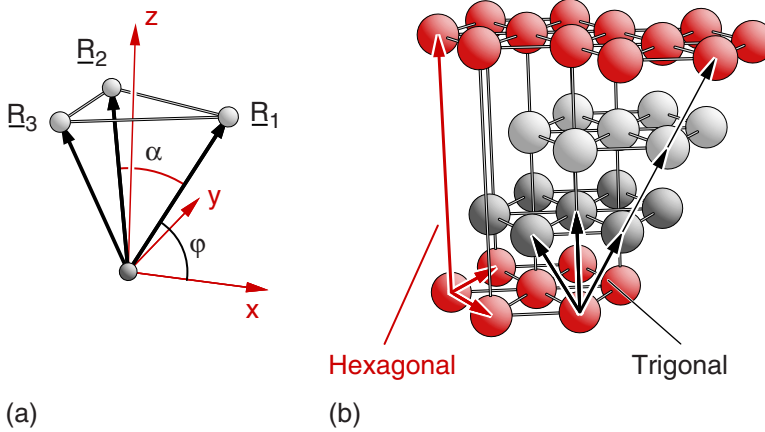


**Figure 2.11** (a) Lattice vectors  $\underline{R}_1$ ,  $\underline{R}_2$ ,  $\underline{R}_3$  of the trigonal (rhombic) lattice with definitions of the Cartesian coordinate system and of angles  $\varphi$ ,  $\alpha$ , see text. (b) Three trigonal lattices combining to form a non-primitive hexagonal lattice. Lattice vectors are shown by arrows, black for trigonal and red for hexagonal. The visual correlation between the two lattices is indicated by thin gray sticks connecting hexagonal lattice points.

$$\cos(\alpha) = \cos(\beta) = \cos(\gamma) = 1/4 \{1 - 3 \cos(2\varphi)\} \quad (2.47)$$

Thus, the three vectors  $\underline{R}'_1$ ,  $\underline{R}'_2$ ,  $\underline{R}'_3$  with

$$\underline{R}'_1 = \underline{R}_1 - \underline{R}_2 = \sqrt{3}c_1a (\sqrt{3}/2, -1/2, 0)$$

$$\underline{R}'_2 = \underline{R}_2 - \underline{R}_3 = \sqrt{3}c_1a (0, 1, 0)$$

$$\underline{R}'_3 = \underline{R}_1 + \underline{R}_2 + \underline{R}_3 = 3c_2a (0, 0, 1) \quad (2.48)$$

form a **hexagonal sublattice** (**obtuse** representation) of the trigonal lattice since

$$|\underline{R}'_1|^2 = |\underline{R}'_2|^2 = 3a^2 \cos^2(\varphi), \quad |\underline{R}'_3|^2 = 9a^2 \sin^2(\varphi)$$

$$\angle(\underline{R}'_1, \underline{R}'_2) = 120^\circ, \quad \angle(\underline{R}'_1, \underline{R}'_3) = \angle(\underline{R}'_2, \underline{R}'_3) = 90^\circ \quad (2.49)$$

(Actually, lattice vectors (2.48) can be easily shown to coincide with definition (2.45a) of a hexagonal lattice by applying a rotation by  $30^\circ$  about the axis through  $\underline{R}'_3$  and a scaling of the lattice constants where constants  $a$  and  $c$  in Eq. (2.45a) correspond to  $(\sqrt{3} c_1 a)$  and  $(3 c_2 a)$  in Eq. (2.48).)

**General lattice points** of the hexagonal sublattice are given according to Eqs. (2.46) and (2.48) by vectors

$$\begin{aligned} \underline{R} &= n_1 \underline{R}'_1 + n_2 \underline{R}'_2 + n_3 \underline{R}'_3 \\ &= (n_1 + n_3) \underline{R}_1 + (n_2 - n_1 + n_3) \underline{R}_2 + (n_3 - n_2) \underline{R}_3 \\ &= m_1 \underline{R}_1 + m_2 \underline{R}_2 + m_3 \underline{R}_3 \end{aligned} \quad (2.50)$$

where the coefficients  $m_i$  and  $n_i$  are connected by linear transformations written in matrix form as

$$\begin{pmatrix} m_1 \\ m_2 \\ m_3 \end{pmatrix} = \begin{pmatrix} 1 & 0 & 1 \\ -1 & 1 & 1 \\ 0 & -1 & 1 \end{pmatrix} \cdot \begin{pmatrix} n_1 \\ n_2 \\ n_3 \end{pmatrix} \quad (2.51a)$$

and

$$\begin{pmatrix} n_1 \\ n_2 \\ n_3 \end{pmatrix} = \frac{1}{3} \begin{pmatrix} 2 & -1 & -1 \\ 1 & 1 & -2 \\ 1 & 1 & 1 \end{pmatrix} \cdot \begin{pmatrix} m_1 \\ m_2 \\ m_3 \end{pmatrix} \quad (2.51b)$$

According to Eq. (2.51b), the hexagonal sublattice is described by integer values  $n_1, n_2, n_3$  only if the corresponding trigonal coefficients  $m_1, m_2, m_3$  fulfill the **three** conditions

$$2 m_1 - m_2 - m_3 = 3g, \quad m_1 + m_2 - 2 m_3 = 3g', \quad m_1 + m_2 + m_3 = 3g'' \quad (2.52)$$

where  $g, g', g''$  are integers. Since

$$m_1 + m_2 + m_3 = (m_1 + m_2 - 2 m_3) + 3 m_3 = -(2 m_1 - m_2 - m_3) + 3 m_1 \quad (2.53)$$

fulfilling one of the three conditions (2.52) will automatically satisfy the other two. Considering the complete trigonal lattice, all sets of coefficients  $m_1, m_2, m_3$  can be grouped according to one of the three categories,

$$m_1 + m_2 + m_3 = 3g \quad (2.54a)$$

$$m_1 + m_2 + m_3 = 3g + 1 \quad \text{or} \quad (m_1 - 1) + m_2 + m_3 = 3g \quad (2.54b)$$

$$m_1 + m_2 + m_3 = 3g + 2 \quad \text{or} \quad (m_1 - 2) + m_2 + m_3 = 3g \quad (2.54c)$$

Here the condition (2.54a) was shown to result in a hexagonal lattice whose origin coincides with that of the trigonal lattice. The conditions of Eq. (2.54b) also lead to a hexagonal lattice. However, its origin is shifted with respect to that of the trigonal lattice by a trigonal lattice vector  $\underline{R}_1$  (or  $\underline{R}_2$  or  $\underline{R}_3$ ). Analogously, the conditions of Eq. (2.54c) lead to an identical hexagonal lattice with its origin shifted by a trigonal lattice vector  $2\underline{R}_1$  (or any combination of two trigonal lattice vectors). Since all lattice points of the trigonal lattice satisfy one of the three conditions (2.54) the **trigonal** lattice can be decomposed into **three** identical **hexagonal** lattices that are shifted with respect to each other as sketched by the thinner arrows in Figure 2.11b.

Altogether, any crystal with a trigonal lattice, given by lattice vectors (2.46), can be alternatively described by a crystal with a non-primitive hexagonal lattice, with lattice vectors (2.48), where the unit cell of the hexagonal lattice contains three times as many atoms compared with that of the trigonal lattice. Further, the lattice vectors  $\underline{R}_1^{\text{hex}}, \underline{R}_2^{\text{hex}}, \underline{R}_3^{\text{hex}}$  of the hexagonal lattice representation are **non-primitive**.

### 2.2.2.2 Superlattices and Repeated Slabs

As mentioned earlier, theoretical studies on the physical or chemical parameters inside a crystal often require considering a unit cell with lattice vectors  $\underline{R}_1, \underline{R}_2, \underline{R}_3$ , which is larger than the primitive cell of the lattice given by  $\underline{R}_{o1}, \underline{R}_{o2}, \underline{R}_{o3}$ . Examples of this so-called **supercell** or **superlattice** concept include spin alignment in antiferromagnetic crystals [45], where the magnetic lattice, defined by positions of the different spins, differs from the geometric lattice of the crystal. In addition, local perturbations, such as vacancies, added atoms, or substituted atoms in alloy formation [46], of otherwise perfect crystals have been examined theoretically [47] applying supercell concepts. Here, single perturbations are simulated by those in an artificial crystal with large supercells such that distances between periodic copies of the perturbations are large enough to avoid physical coupling. Further, small distortions of lattice positions, which can result in periodicity with large supercells have been considered in so-called frozen phonon calculations [48]. Finally, we mention the use of supercell geometry in calculations of physical and chemical properties of single crystal surfaces. These calculations are often based on the so-called **repeated slab geometry** [48], where the surface region is approximated by a slab of finite thickness and a vacuum gap repeated periodically such that overall a three-dimensional periodicity with a large supercell is achieved.

The basic **mathematical** idea behind **conventional** supercell descriptions relies on the fact that any crystal with a lattice described by primitive lattice vectors  $\underline{R}_{o1}, \underline{R}_{o2}, \underline{R}_{o3}$  and an atom basis can be represented by an alternative (non-primitive) lattice with (larger) lattice vectors  $\underline{R}_1, \underline{R}_2, \underline{R}_3$  and an appropriately modified basis. The alternative vectors are connected with those of the initial lattice by a linear transformation that must be integer-valued if the global three-dimensional periodicity is to be conserved. This can be expressed mathematically by a **transformation matrix**  $\underline{T}$  with

$$\begin{pmatrix} \underline{R}_1 \\ \underline{R}_2 \\ \underline{R}_3 \end{pmatrix} = \begin{pmatrix} t_{11} & t_{12} & t_{13} \\ t_{21} & t_{22} & t_{23} \\ t_{31} & t_{32} & t_{33} \end{pmatrix} \cdot \begin{pmatrix} \underline{R}_{o1} \\ \underline{R}_{o2} \\ \underline{R}_{o3} \end{pmatrix} = \underline{T} \cdot \begin{pmatrix} \underline{R}_{o1} \\ \underline{R}_{o2} \\ \underline{R}_{o3} \end{pmatrix} \quad (2.55)$$

where the elements  $t_{ij}$  of matrix  $\underline{T}$  are integers. As a consequence, the volumes  $V_{el}$  and  $V_{el}^o$  of the unit cells of the two lattices, defined by Eq. (2.9), are connected by

$$V_{el} = |(\underline{R}_1 \times \underline{R}_2) \cdot \underline{R}_3| = |\det(\underline{T})| |(\underline{R}_{o1} \times \underline{R}_{o2}) \cdot \underline{R}_{o3}| = |\det(\underline{T})| V_{el}^o \quad (2.56)$$

where Eq. (2.55) together with vector relation (F.9) of Appendix F is applied. This means, in particular, that the volume  $V_{el}$  of the supercell must be an integer multiple of volume  $V_{el}^o$  of the initial unit cell.

In the simplest case, the superlattice description results from simple **scaling** of the initial lattice vectors, corresponding to a transformation

$$\underline{R}_1 = m_1 \underline{R}_{o1}, \quad \underline{R}_2 = m_2 \underline{R}_{o2}, \quad \underline{R}_3 = m_3 \underline{R}_{o3} \quad (2.57)$$

with integer-valued  $m_1, m_2, m_3$ . Thus, the transformation matrix  $\underline{\mathbb{T}}$  becomes diagonal, that is,

$$\underline{\mathbb{T}} = \begin{pmatrix} m_1 & 0 & 0 \\ 0 & m_2 & 0 \\ 0 & 0 & m_3 \end{pmatrix} \quad (2.58)$$

As an **illustration**, we consider a fictitious sc crystal with ferromagnetic and anti-ferromagnetic ordering of its atoms, where the antiferromagnetism introduces a doubling of the lattice vectors in two dimensions, as sketched in Figure 2.12. Thus, the lattice vectors of the antiferromagnetic crystal,  $\underline{R}_1, \underline{R}_2, \underline{R}_3$ , can be connected with those of the ferromagnetic crystal,  $\underline{R}_{o1}, \underline{R}_{o2}, \underline{R}_{o3}$ , by

$$\underline{R}_1 = 2 \underline{R}_{o1}, \quad \underline{R}_2 = 2 \underline{R}_{o2}, \quad \underline{R}_3 = \underline{R}_{o3} \quad (2.59)$$

Theoretical studies of the antiferromagnetic crystal must be based on a lattice description given by  $\underline{R}_1, \underline{R}_2, \underline{R}_3$  while studies of the ferromagnetic crystal allow the use of the smaller lattice vectors  $\underline{R}_{o1}, \underline{R}_{o2}, \underline{R}_{o3}$ . However, a direct comparison of physical properties of the two crystals with different spin alignments can be simplified by using identical lattice parameters, which suggests applying the superlattice vectors  $\underline{R}_1, \underline{R}_2, \underline{R}_3$  also for the ferromagnetic crystal.

Incidentally, Figure 2.12 shows that, for the present sc crystal with its antiferromagnetic spin alignment, alternative lattice vectors  $\underline{R}'_1, \underline{R}'_2, \underline{R}'_3$  with

$$\underline{R}'_1 = 1/2 (\underline{R}_1 + \underline{R}_2), \quad \underline{R}'_2 = 1/2 (\underline{R}_2 - \underline{R}_1), \quad \underline{R}'_3 = \underline{R}_3 \quad (2.60)$$

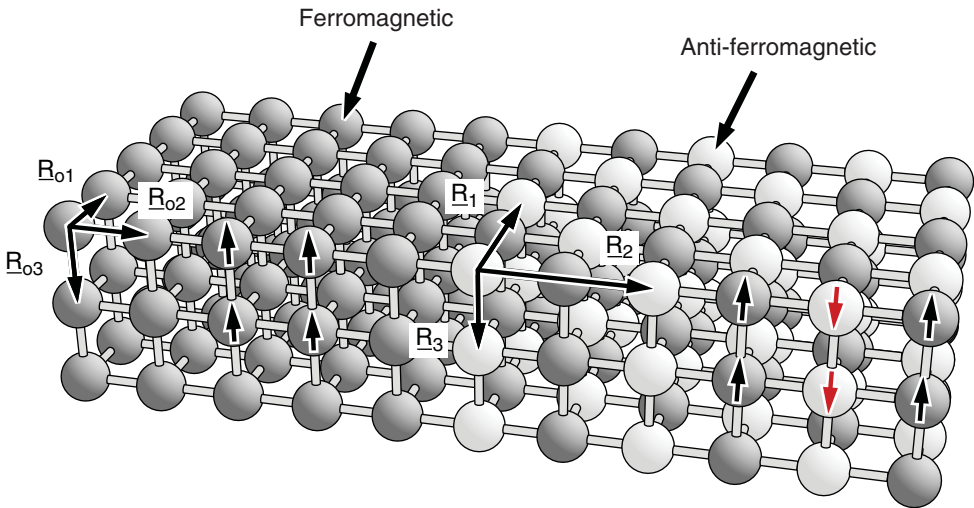


**Figure 2.12** Fictitious sc crystal with ferromagnetic (left) and anti-ferromagnetic ordering (right). Atoms are shown as dark (spin up) and light (spin down) balls with their spin orientation indicated by black and red arrows. The superlattice vectors  $\underline{R}_1, \underline{R}_2, \underline{R}_3$  and primitive lattice vectors  $\underline{R}_{o1}, \underline{R}_{o2}, \underline{R}_{o3}$  are labeled accordingly.

could also be chosen, yielding a smaller morphological unit cell than that given by Eq. (2.59). This vector set can also be used to describe a superlattice of the ferromagnetic crystal.

As mentioned earlier, computational studies of the physical and chemical properties of single crystal surfaces are often based on the so-called **repeated slab geometry** [48], which can be considered a **modified** supercell concept. Within this concept a single crystal with a confining planar surface of given orientation and periodicity is described approximately by a two-dimensionally periodic solid layer of finite thickness (**slab**) cut out of the bulk crystal. Here, two bulk lattice vectors,  $\underline{R}_1$  and  $\underline{R}_2$ , characterize the two-dimensional periodicity of the surface (and that of the slab). In addition, the slab is repeated periodically along the direction of its surface normal with a vacuum gap between adjacent slabs where the periodicity vector  $\underline{R}_3$  is chosen appropriately. This procedure creates an altogether three-dimensionally periodic crystal system with a **fictitious** superlattice

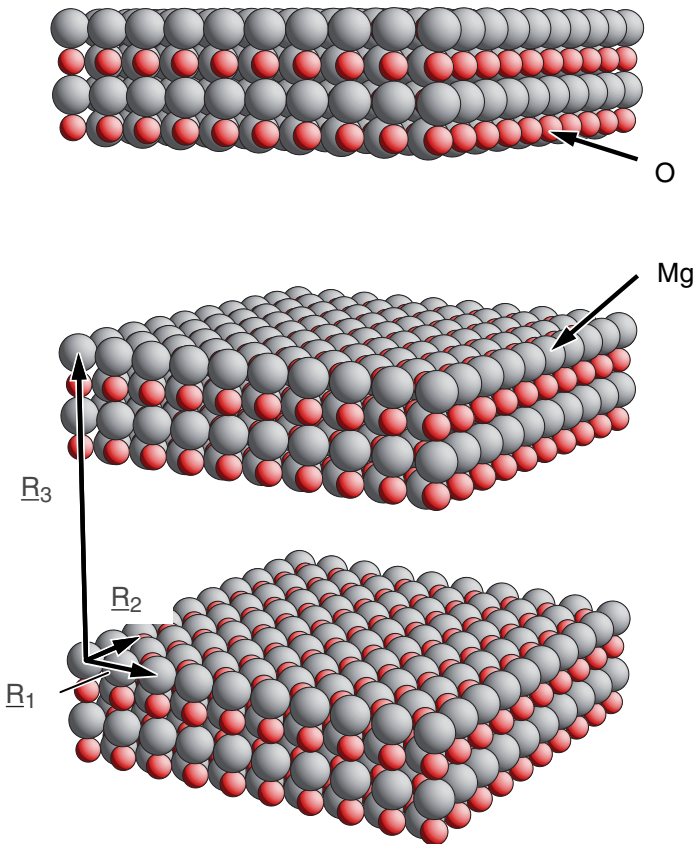


**Figure 2.13** Structure of MgO substrate confined by  $(1\ 0\ 0)$  and  $(-1\ 0\ 0)$  oriented surfaces in repeated slab geometry (three slabs). The superlattice vectors  $\underline{R}_1$ ,  $\underline{R}_2$ ,  $\underline{R}_3$  are labeled accordingly.

$\underline{R}_1$ ,  $\underline{R}_2$ ,  $\underline{R}_3$ , which is connected with the initial crystal lattice only by vectors  $\underline{R}_1$  and  $\underline{R}_2$ . As a result, matrix  $\underline{T}$  of Eq. (2.55) contains integer-valued elements in its first and second rows while its third row may be real-valued. Within the **repeated slab** concept, the physical and chemical parameters of crystalline surfaces can be evaluated by well-established computational methods developed a long time ago for three-dimensionally periodic bulk crystals in solid state physics. For this approach to be meaningful the slabs must be sufficiently thick so that the surfaces of their upper and lower sides are electronically decoupled. Further, the vacuum distance between neighboring slabs must be sufficiently large such that they do not influence each other electronically.

As an illustration, Figure 2.13 shows three slabs of a magnesium oxide crystal confined by (1 0 0) and  $(-1\ 0\ 0)$  oriented surfaces at their tops and bottoms consisting of four MgO layers each with a vacuum separation of about three times the slab thickness. The appropriate superlattice vectors  $\underline{R}_1$ ,  $\underline{R}_2$ ,  $\underline{R}_3$ , referring to a  $2 \times 2$  supercell laterally, that is, along  $\underline{R}_1$  and  $\underline{R}_2$ , are sketched and labeled accordingly. The size of the supercell is much larger than that of the bulk crystal and the number of atoms in the cell,  $4 \times 8 = 32$  in the present model structure, is rather large compared with that of the primitive bulk containing two atoms. Therefore, computational studies applying the repeated slab geometry are usually much more demanding than those of the corresponding bulk crystal.

As another illustration, Figure 2.14 shows a more complicated structure of three slabs of an fcc silver crystal confined by kinked surfaces (denoted (12 11 7) and  $(-12\ -11\ -7)$ , respectively) at their top and bottom with a vacuum separation corresponding to four times the slab thickness. Again, the appropriate superlattice vectors  $\underline{R}_1$ ,  $\underline{R}_2$ ,  $\underline{R}_3$  show that the size of the supercell with 25 atoms is much larger than the primitive cell of the bulk crystal with one atom only, demonstrating the difference in computational effort between slab and bulk calculations.

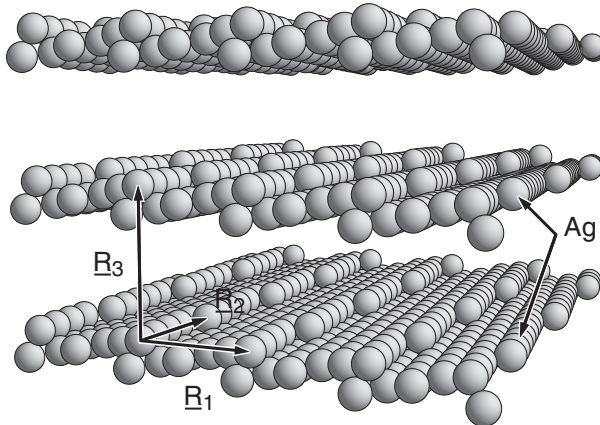


**Figure 2.14** Structure of silver substrate confined by (12 11 7) and  $(-12\ -11\ -7)$  oriented surfaces in repeated slab geometry (three slabs). The superlattice vectors  $\underline{R}_1$ ,  $\underline{R}_2$ ,  $\underline{R}_3$  are labeled accordingly.

### 2.2.2.3 Linear Transformations of Lattice Vectors

One group of alternative descriptions of crystal lattices is given by those where the alternative lattice vectors  $\underline{R}_1, \underline{R}_2, \underline{R}_3$  are **linear combinations** of their initial counterparts  $\underline{R}_{o1}, \underline{R}_{o2}, \underline{R}_{o3}$  with integer coefficients. This was already discussed in connection with the superlattice concept, and the basic linear transformation was defined by Eq. (2.55). Among these alternatives, there are lattice descriptions, whose morphological unit cells change their shape but not their volume, when compared with those of the initial lattice.

The latter alternatives can be used in practical cases to **adapt** the lattice description of a single crystal to additional **geometric constraints**, in particular those introduced by the existence of a single crystal surface. Therefore, these alternative descriptions are important for a crystallographic characterization of single crystal surfaces, as will become more evident in Chapters 4 and 5. In addition, they can be used to adapt lattice descriptions such that symmetry elements of the lattice become easily visible. As a simple example in two dimensions, Figure 2.15 shows two alternative descriptions of the square lattice by lattice vectors  $\underline{R}_{o1}, \underline{R}_{o2}$  and  $\underline{R}_1, \underline{R}_2$ , respectively, where the two sets are connected by a linear transformation

$$\underline{R}_1 = -\underline{R}_{o1} - \underline{R}_{o2}, \quad \underline{R}_2 = 2\underline{R}_{o1} + \underline{R}_{o2} \quad (2.61)$$

Both vector sets,  $\underline{R}_{o1}, \underline{R}_{o2}$  and  $\underline{R}_1, \underline{R}_2$ , provide mathematically exact descriptions of the square lattice and form morphological unit cells of the same volume. However, lattice vectors  $\underline{R}_{o1}, \underline{R}_{o2}$  are of the same length and perpendicular to each other. Thus, their unit cell reveals additional symmetry properties of the lattice, such as mirror and rotational symmetry.

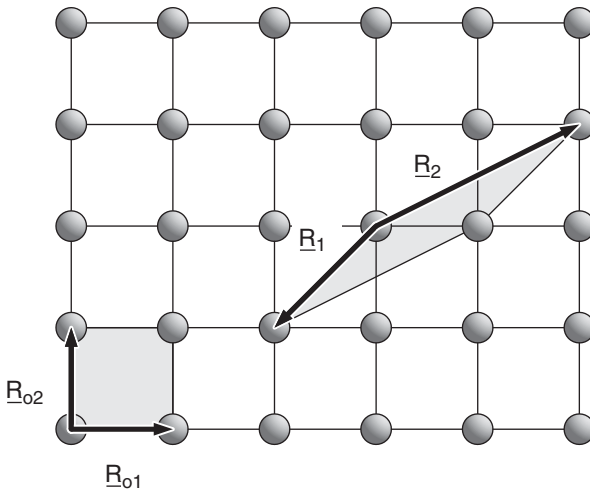


**Figure 2.15** Alternative description of the square lattice by lattice vectors  $\underline{R}_{o1}, \underline{R}_{o2}$  and  $\underline{R}_1, \underline{R}_2$ , respectively. The morphological unit cells of the two descriptions are emphasized by gray painting.

In the **general case**, we consider lattice vectors  $\underline{R}_1, \underline{R}_2, \underline{R}_3$  of an alternative lattice description as a result of a linear transformation applied to an initial set of lattice vectors  $\underline{R}_{o1}, \underline{R}_{o2}, \underline{R}_{o3}$ , which according to Eq. (2.55) can be written in matrix form as

$$\begin{pmatrix} \underline{R}_1 \\ \underline{R}_2 \\ \underline{R}_3 \end{pmatrix} = \begin{pmatrix} t_{11} & t_{12} & t_{13} \\ t_{21} & t_{22} & t_{23} \\ t_{31} & t_{32} & t_{33} \end{pmatrix} \cdot \begin{pmatrix} \underline{R}_{o1} \\ \underline{R}_{o2} \\ \underline{R}_{o3} \end{pmatrix} = \underline{\mathbb{T}} \cdot \begin{pmatrix} \underline{R}_{o1} \\ \underline{R}_{o2} \\ \underline{R}_{o3} \end{pmatrix} \quad (2.62)$$

If the lattice vectors  $\underline{R}_1, \underline{R}_2, \underline{R}_3$  are to describe the same set of lattice points as vectors  $\underline{R}_{o1}, \underline{R}_{o2}, \underline{R}_{o3}$ , then a general lattice point at  $\underline{R}$  must be representable by an integer-valued linear combination of both sets of lattice vectors, that is,

$$\underline{R} = n_{o1} \underline{R}_{o1} + n_{o2} \underline{R}_{o2} + n_{o3} \underline{R}_{o3} = n_1 \underline{R}_1 + n_2 \underline{R}_2 + n_3 \underline{R}_3, \quad n_{oi}, n_i \text{ integer} \quad (2.63)$$

Thus, any triplet of integers  $n_1, n_2, n_3$  corresponds to another integer triplet  $n_{o1}, n_{o2}, n_{o3}$  and vice versa. This means, in particular, that the transformation matrix  $\underline{\mathbb{T}} = (t_{ij})$  in Eq. (2.62) must be **integer-valued**. Further, transformation (2.62) can be inverted to yield

$$\begin{pmatrix} \underline{R}_{o1} \\ \underline{R}_{o2} \\ \underline{R}_{o3} \end{pmatrix} = \begin{pmatrix} t'_{11} & t'_{12} & t'_{13} \\ t'_{21} & t'_{22} & t'_{23} \\ t'_{31} & t'_{32} & t'_{33} \end{pmatrix} \cdot \begin{pmatrix} \underline{R}_1 \\ \underline{R}_2 \\ \underline{R}_3 \end{pmatrix} = \underline{\mathbb{T}}^{-1} \cdot \begin{pmatrix} \underline{R}_1 \\ \underline{R}_2 \\ \underline{R}_3 \end{pmatrix} \quad (2.64)$$

where the matrix elements  $t'_{ij}$  of the inverse matrix  $\underline{\mathbb{T}}^{-1}$  also must be integers. Since all elements of  $\underline{\mathbb{T}}$  are integers the determinant of matrix  $\underline{\mathbb{T}}$ , given by

$$\det(\underline{\mathbb{T}}) = t_{11} (t_{22} t_{33} - t_{23} t_{32}) + t_{12} (t_{23} t_{31} - t_{21} t_{33}) + t_{13} (t_{21} t_{32} - t_{22} t_{31}) \quad (2.65)$$

must be integer-valued. The same must be true for the inverse matrix  $\underline{\mathbb{T}}^{-1}$ . From linear algebra, we know that

$$\det(\underline{\mathbb{T}}^{-1}) = 1/\det(\underline{\mathbb{T}}) \quad (2.66)$$

Thus, both determinant values must be non-zero integers, that is,  $|\det(\underline{\mathbb{T}})| \geq 1$  and  $|\det(\underline{\mathbb{T}}^{-1})| \geq 1$ , which according to Eq. (2.66) can only be possible if

$$\det(\underline{\mathbb{T}}) = \det(\underline{\mathbb{T}}^{-1}) = \pm 1 \quad (2.67)$$

Here the determinant value  $-1$  can be safely ignored since it affects only the sequence in which the lattice vectors appear in the transformation (connected with handedness of the vector set). Any transformation Eq. (2.62) with  $\det(\underline{\mathbb{T}}) = -1$  can be modified to yield  $\det(\underline{\mathbb{T}}) = 1$  by exchanging one vector pair  $\underline{R}_i, \underline{R}_j$  in the transformation.

Relation (2.67) imposes a **constraint** to possible transformation matrices  $\underline{\mathbb{T}}$ . Combining Eq. (2.67) with Eq. (2.65) one can write

$$\det(\underline{\mathbb{T}}) = a_1 t_{11} + a_2 t_{12} + a_3 t_{13} = 1 \quad (2.68)$$

with integer-valued coefficients  $a_i$  where

$$\begin{aligned} a_1 &= t_{22}t_{33} - t_{23}t_{32} \\ a_2 &= t_{23}t_{31} - t_{21}t_{33} \\ a_3 &= t_{21}t_{32} - t_{22}t_{31} \end{aligned} \quad (2.69)$$

Equation (2.68) represents a linear Diophantine equation containing only integers as parameters and variables. As shown in Appendix E.3, this equation has integer solutions  $a_1, a_2, a_3$  for given  $t_{11}, t_{12}, t_{13}$  only if the latter three numbers have no common divisor greater than 1. Thus, the transformed lattice vector

$$\underline{R}_1 = t_{11}\underline{R}_{o1} + t_{12}\underline{R}_{o2} + t_{13}\underline{R}_{o3} \quad (2.70)$$

is of **smallest length** along its direction in the lattice. Rearranging the components in the determinant (2.65) we can easily derive analogous relations

$$\det(\underline{T}) = b_1t_{21} + b_2t_{22} + b_3t_{23} = 1 \quad (2.71)$$

$$\det(\underline{T}) = c_1t_{31} + c_2t_{32} + c_3t_{33} = 1 \quad (2.72)$$

with integer-valued coefficients  $b_i, c_i$ , where

$$\begin{aligned} b_1 &= t_{32}t_{13} - t_{12}t_{33}, & c_1 &= t_{12}t_{23} - t_{13}t_{22} \\ b_2 &= t_{33}t_{11} - t_{13}t_{31}, & c_2 &= t_{13}t_{21} - t_{11}t_{23} \\ b_3 &= t_{31}t_{12} - t_{11}t_{32}, & c_3 &= t_{11}t_{22} - t_{12}t_{21} \end{aligned} \quad (2.73)$$

Then the corresponding linear Diophantine equations (2.71) and (2.72) have integer solutions  $b_1, b_2, b_3$  for given  $t_{21}, t_{22}, t_{23}$  (and  $c_1, c_2, c_3$  for given  $t_{31}, t_{32}, t_{33}$ ) only if the latter three numbers have no common divisor greater than 1. Thus, the transformed lattice vectors

$$\underline{R}_2 = t_{21}\underline{R}_{o1} + t_{22}\underline{R}_{o2} + t_{23}\underline{R}_{o3} \quad (2.74)$$

$$\underline{R}_3 = t_{31}\underline{R}_{o1} + t_{32}\underline{R}_{o2} + t_{33}\underline{R}_{o3} \quad (2.75)$$

are also of **smallest length** along their direction in the lattice.

### 2.2.3

#### Centered Lattices

In Section 2.2.2.1 it was shown that the bcc lattice, characterizing, for example, iron single crystals, see Figure 2.16a, can be described by non-primitive lattice vectors  $\underline{R}_1, \underline{R}_2, \underline{R}_3$  that form an sc lattice. However, there is an additional lattice vector  $\underline{R}'$  inside the morphological unit cell, spanned by  $\underline{R}_1, \underline{R}_2, \underline{R}_3$ , which points to the center of the cubic unit cell, as illustrated in Figure 2.16b. This is an example of a more general property of non-primitive lattice representations, commonly denoted as **centering** and discussed in the following.